NAVAL POSTGRADUATE SCHOOL

MONTEREY, CALIFORNIA

THESIS

ANALYTICAL MODELING OF COMPOSITE-TO-COMPOSITE (SCARF) JOINTS IN TENSION AND COMPRESSION

by

Todd R. Greene

June 2007

Thesis Advisor:	Young W. Kwon
Second Reader:	Scott W. Bartlett

Approved for public release; distribution is unlimited.

THIS PAGE INTENTIONALLY LEFT BLANK

REPORT DOCUMENTATION PAGE		*Form Approved OMB No. 0704-0188*
Public reporting burden for this collection of information is estimated to average 1 hour per response, including the time for reviewing instruction, searching existing data sources, gathering and maintaining the data needed, and completing and reviewing the collection of information. Send comments regarding this burden estimate or any other aspect of this collection of information, including suggestions for reducing this burden, to Washington headquarters Services, Directorate for Information Operations and Reports, 1215 Jefferson Davis Highway, Suite 1204, Arlington, VA 22202-4302, and to the Office of Management and Budget, Paperwork Reduction Project (0704-0188) Washington DC 20503.

1. AGENCY USE ONLY *(Leave blank)*	**2. REPORT DATE** June 2007	**3. REPORT TYPE AND DATES COVERED** Master's Thesis
4. TITLE AND SUBTITLE Analytical Modeling of Composite-to-Composite (Scarf) Joints in Tension and Compression		**5. FUNDING NUMBERS**
6. AUTHOR(S) Todd R. Greene		
7. PERFORMING ORGANIZATION NAME(S) AND ADDRESS(ES) Naval Postgraduate School Monterey, CA 93943-5000		**8. PERFORMING ORGANIZATION REPORT NUMBER**
9. SPONSORING /MONITORING AGENCY NAME(S) AND ADDRESS(ES) N/A		**10. SPONSORING/MONITORING AGENCY REPORT NUMBER**
11. SUPPLEMENTARY NOTES The views expressed in this thesis are those of the author and do not reflect the official policy or position of the Department of Defense or the U.S. Government.		
12a. DISTRIBUTION / AVAILABILITY STATEMENT Approved for public release; distribution is unlimited.		**12b. DISTRIBUTION CODE** A

13. ABSTRACT

Fracture mechanics-based multi-level computational modeling and simulation techniques were developed to predict failure strengths of composite scarf joints under tension or compression. Global, local, and element level models were used in the study in order to calculate the energy release rates at the scarf joints. The study showed that explicit modeling of the resin layer at the scarf joint, where cracks initiate, was important for accurate prediction of the joint failure strengths. In addition, the consideration of the joint interface slope in the fracture model was important especially for compressive joint failure strengths. In terms of the mixed failure criteria for crack propagation, the interactive biquadratic criterion was found to be useful for reliable prediction of joint failure strengths. The predicted strengths were in good agreement with experimental data which were obtained for two different kinds of polymer composites, e-glass/epoxy or carbon/epoxy.

14. SUBJECT TERMS scarf joint, composite, finite element method, fracture criteria			**15. NUMBER OF PAGES** 87
			16. PRICE CODE
17. SECURITY CLASSIFICATION OF REPORT Unclassified	**18. SECURITY CLASSIFICATION OF THIS PAGE** Unclassified	**19. SECURITY CLASSIFICATION OF ABSTRACT** Unclassified	**20. LIMITATION OF ABSTRACT** UL

THIS PAGE INTENTIONALLY LEFT BLANK

**ANALYTICAL MODELING OF COMPOSITE-TO-COMPOSITE (SCARF)
JOINTS IN TENSION AND COMPRESSION**

Todd R. Greene
Lieutenant, United States Navy
B.S., United States Naval Academy, 1999

Submitted in partial fulfillment of the
requirements for the degree of

MASTER OF SCIENCE IN MECHANICAL ENGINEERING

from the

**NAVAL POSTGRADUATE SCHOOL
June 2007**

Author: Todd R. Greene

Approved by: Young Kwon
                 Thesis Advisor

                 Scott Bartlett
                 Second Reader

                 Anthony Healey
                 Chairman, Department of Mechanical and Astronautical
                 Engineering

THIS PAGE INTENTIONALLY LEFT BLANK

ABSTRACT

Fracture mechanics-based multi-level computational modeling and simulation techniques were developed to predict failure strengths of composite scarf joints under tension or compression. Global, local, and element level models were used in the study in order to calculate the energy release rates at the scarf joints. The study showed that explicit modeling of the resin layer at the scarf joint, where cracks initiate, was important for accurate prediction of the joint failure strengths. In addition, the consideration of the joint interface slope in the fracture model was important especially for compressive joint failure strengths. In terms of the mixed failure criteria for crack propagation, the interactive biquadratic criterion was found to be useful for reliable prediction of joint failure strengths. The predicted strengths were in good agreement with experimental data which were obtained for two different kinds of polymer composites, e-glass/epoxy or carbon/epoxy.

THIS PAGE INTENTIONALLY LEFT BLANK

TABLE OF CONTENTS

THIS PAGE INTENTIONALLY LEFT BLANK

LIST OF FIGURES

THIS PAGE INTENTIONALLY LEFT BLANK

LIST OF TABLES

THIS PAGE INTENTIONALLY LEFT BLANK

ACKNOWLEDGMENTS

THIS PAGE INTENTIONALLY LEFT BLANK

I.   INTRODUCTION

A.   BACKGROUND

Composite structures consist of fiber reinforcements (such as E-glass or carbon) encapsulated in a resin matrix (such as vinyl ester). Composite materials can be used to produce a variety of structures. In maritime applications, composites, specifically glass reinforced plastics (GRP), have been used for primary structures in small craft for the past several decades. In larger, steel vessels, composites have also found applications but only in secondary structures such as decks, foundations, doors, hatch covers, stacks, and masts.   The difficulty of creating a strong joint between two independently molded composite sections has limited any applications beyond secondary structures in large vessels. One of the largest hurdles preventing widespread incorporation of composites in modern ship construction remains the risk involved in joining two pre-formed sections. Composites are often deemed an unsuitable material choice for parts that are too large to be formed in one mold, in a single lay-up, due to the weakness and uncertainty about the joint. Therefore, weldable metals, where the process of joining two sections is very well understood, remain the primary type of ship building material.

Currently, the decreasing price and increasing availability of advanced composite materials, as well as their superior mechanical properties, are causing the maritime industry to renew its interest in applying composite materials for primary structures in ship construction. Today's lack of understanding regarding composite joints often causes marine composite applications to be over designed, or it requires expensive experimental testing to be undertaken to mitigate the risk involved with the lesser understood joints. In order to pass this hurdle and allow composites to rival steel and aluminum in large marine structures, advancement in the understanding of the mechanics of composite joints is required.

B. LITERATURE REVIEW

1. Advantages of Composites in Ship Construction

Composites offer many advantages to standard metallic structures. Below is a summary of the advantages as detailed by the Naval Surface Warfare Center, Carderock Division (NSWCCD) in their High-Speed Sealift Technology Development Plan: [1]

1. Composites are light weight. Weight reductions of 35 to 50 %, compared to steel, can currently be realized for secondary structures made of E-glass composite laminates. Since secondary structures comprise a significant fraction of the total structural weight, this translates to a total ship weight savings of about 8 percent of a large vessel (nominally 800 feet long).

2. Composite structural elements have better dimensional stability than steel elements. This is an aid to the fit-up and assembly in the shipyard, and results in lower fabrication costs and better overall dimensional tolerances.

3. They have reduced noise and vibration properties. Composites have inherently better damping and compliance than metallic structures. They also have the potential to be adapted into smart structures, i.e., structures that can monitor and/or adapt their properties in service.

4. Fires are more easily contained in composite structures because of their low thermal conductivity. The cores in composite sandwich panels are good thermal insulators.

5. The designer has increased flexibility to tailor the composite structure to the particular need. Complex geometries can be designed to optimize the strength and stiffness, or to enhance the producibility by minimizing the number or location of joints.

6. Composites have lower life-cycle maintenance costs than steel structures. Fewer inspections, less painting, and fewer repairs are needed over the life of the ship because of the non-corrosion and reduced fatigue damage of composites over metallic structures.

Composites are more advantageous than steel or aluminum when compared on an equivalent strength basis rather then on stiffness basis. The relative weights of panels having equal stiffness and equal strength under both in-plane (axial) and bending loads presented at the Second International Conference Marine Applications of Composite Materials are listed in Tables 1 through 5, in Appendix A. [2]

2. Specifics of the Scarf Joint

One simple, but important, type of composite joint is the scarf joint. Scarf joints are typically used to connect separate sections of large solid-laminate composite structure while maintaining a constant laminate thickness. This way, large structures are divided into more easily manufactured sections, with minimal structural losses, and without introducing more complicated joints. A drawback with the scarf joint is the reduced strength of the secondary bond (bonding to something that has already cured) when one section is infused onto a previously manufactured section. Figure 1 depicts a typical scarf joint. The area on the left (dark grey) represents the section that was manufactured first. The lighter grey on the right shows the newer material that was joined to the existing structure. [3]
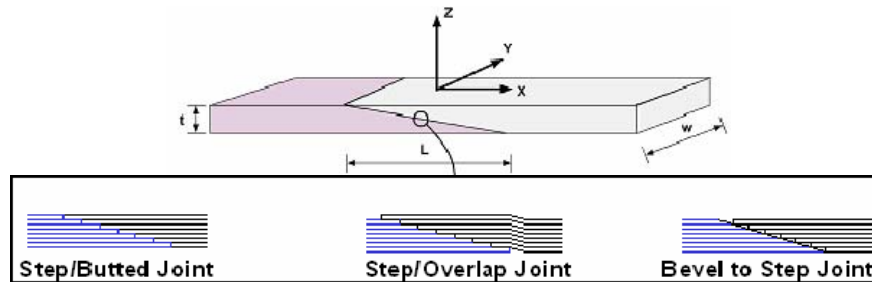
Figure 1.   Scarf Joint Specimen and Manufacturing Options (from Ref [4])

A scarf joint is an applicable technique whenever it is necessary to add a new section of material to an existing structure. A scarf joint can be used by a shipyard during initial fabrication, and it can also be used during operation if there is a need to remove and repair damaged material, or add new structure to increase functionality. During fabrication, the scarf joint technique allows an incremental building process where new structure is added to an existing assembly, or when two existing assemblies need to be joined together. As mentioned in the introduction, joining large composite sections is currently a major drawback to using composites in large marine structures.

Figure 2.   Scarf joint being used to joint large composite sections of the Swedish Visby class corvette. (from Ref [4])

Joining solid laminate sections using a scarf technique is a relatively simple concept, however, there are several variables that are involved. When choosing how to join two sections, the designer must consider the following cases: [5]

- Scarf Geometry (L/t ratio, see Figure 1)
- Scarf Configuration (step/butted, step/overlap, bevel to step)
- Surface Preparation
- Time between primary and secondary curing
- Material Selection
- Material Lay-up Technique (VARTM, hand lay-up, etc.)

The effect each of these variables has on the joint needs to be understood so that the best possible solution can be applied for a particular application.

3.   NSWCCD Post-Test Analysis of Composite Scarf Joints

As a starting point for this research, the analysis done by Taylor and Bonanni at NSWCCD [6] provided a starting point for developing the finite element models in this report. Their findings were employed as a base line for model construction, and the detailed exploration of modeling techniques for scarf joints found in this report are based on their recommendations for future work.

C. PURPOSE OF THIS RESEARCH

For this thesis, several parameters affecting the mechanics within a scarf joint were examined. First, analytical models were developed using the finite element technique for a stepped-lap scarf joint within an e-glass/vinyl ester composite panel. Two different panel thicknesses and two different scarf ratios (L/t) where examined. These models were validated by comparison with existing experimental results provided by NSWCCD. Once validated, the models were applied to predict failure loads of scarf joints within panels that were constructed with materials intended for future applications (carbon fiber/vinyl ester).

Extensive and costly risk mitigation testing of composite joints has been a part of every major composite structures program. The goal of this thesis is to provide a better understanding of the mechanics within the joint, so future designers can apply these findings to optimize future composite joints, and thereby minimize the amount of experimental testing required.

D. FUTURE APPLICATIONS

1. DDG-1000 Deck House

The Naval Sea Systems Command (NAVSEA) and the Office of Naval Research (ONR) have been investigating composite materials and structures for several decades to reduce the risk associated with utilizing advanced composite materials. Recent fleet applications have included the composite masts on the DD-968, CVN-77 and the entire LPD-17 fleet. Additionally, the deckhouse of the U.S. Navy's next generation surface ship, the DDG-1000 Zumwalt class destroyer, is currently being designed with composite materials. Both the ONR 6.2 Basic Research (which is funding this work) and the NAVSEA 6.3 Applied Research (Integrated Topside Design Project) are conducting research in joint design and analysis that will impact current and future ship designs. The research described in this thesis will directly contribute to a better understanding of the mechanics within a composite scarf joint.

THIS PAGE INTENTIONALLY LEFT BLANK

II. FAILURE LOAD MODELING

A. CRACK CLOSURE TECHNIQUE

Fracture analysis using the crack closure (CC) method provides the capability to predict through-thickness failure modes and ultimate failure strength in composites. By using the finite element modeling technique, specific forces and displacements can be calculated at the tip of an assumed crack. Linear elastic fracture mechanics are then applied to determine the energy release rate (ERR) of the crack. The ERR values obtained can be compared with the known fracture toughness of the material system (obtained experimentally) to predict the load at which the crack will grow. Spontaneous crack growth quickly leads to release of all the energy stored and material failure.

1. Two-dimensional Fracture Analysis

a. *Assumed Initial Crack Length*

The crack closure method requires an assumed initial flaw to be built into a finite element (FE) model. The length of this flaw is not typically known, so often the flaw is assumed to be just less than what is detectable by inspection. "Undetectable" lengths commonly vary from 0.005 inch to 0.1 inch. For this research, the assumed crack length was set at 0.01 inch (0.0254 cm) for all models. This decision was based on NSWCCD research that found this length to yield the most accurate results when modeling scarf joints of all varieties applicable in this thesis. [7]

b. *Crack Closure Process*

The following is a brief overview of the CC process for determining the energy release rates in both Mode I (opening) and Mode II (shearing), G_I and G_{II}, at the crack tip. A more detailed description of the procedure is published elsewhere. [8] ERRs can be calculated from FE data using equations (1) and (2), below, where F is the force at the crack tip, Δu is the relative displacement of former interfaces caused by the crack opening, and Δa is increment of crack growth.

$$G_I = \frac{1}{2} F_y \frac{\Delta u_y}{\Delta a} \qquad\qquad (1)$$

$$G_{II} = \frac{1}{2} F_x \frac{\Delta u_x}{\Delta a} \qquad\qquad (2)$$

The direction parallel to the crack is indicated by x, and y is the direction perpendicular to the crack. Once the energy release rates applied in the model (for both Mode I and Mode II) are known, they can be compared with known critical ERRs, and the failure load can be predicted.

2. Predicting Failure with Crack Closure Methods

a. *Fracture Failure Criteria*

The Energy Release Rate of a material can be predicted within a finite element model by comparing the nodal forces needed to hold a crack closed with the amount that crack opens once that force is removed. Several fracture failure criteria are commonly considered to predict the interaction between Mode I and Mode II in failure. The most common criteria include: Mode I, Mode II, mixed linear, and mixed quadratic. For this research, bilinear was also considered, and interactive biquadratic will be introduced. Each criterion is shown in its respective order in equations (3) through (9).

$$\frac{G_I}{G_{Ic}} = 1 \qquad\qquad \text{(Mode I)} \qquad\qquad (3)$$

$$\frac{G_{II}}{G_{IIc}} = 1 \qquad\qquad \text{(Mode II)} \qquad\qquad (4)$$

$$\frac{G_I}{G_{Ic}} + \frac{G_{II}}{G_{IIc}} = 1 \qquad\qquad \text{(Mixed Linear)} \qquad\qquad (5)$$

$$\left(\frac{G_I}{G_{Ic}}\right)^2 + \left(\frac{G_{II}}{G_{IIc}}\right)^2 = 1 \qquad \text{(Mixed Quadratic)} \qquad\qquad (6)$$

Bilinear: The criterion depends on the arbitrary parameters ζ and ξ, which are the slopes of the two line segments (see Figure 3) and is written in terms of mixed mode values. [9]

$$G_{Ic}^m = \xi\, G_{IIc}^m + G_{Ic} \tag{7}$$

$$G_{Ic}^m = \zeta\, G_{IIc}^m - \zeta G_{IIc} \tag{8}$$

<div align="center">Interactive Biquadratic:</div>

$$\left(\frac{G_I}{G_{Ic}}\right)^2 + m\left(\frac{G_I}{G_{Ic}}\right)\left(\frac{G_{II}}{G_{IIc}}\right) + \left(\frac{G_{II}}{G_{IIc}}\right)^2 = 1 \tag{9}$$

b.   *Determining Failure Load from Fracture Criteria*

Because the ERR scales with the square of the applied load, the fracture failure criteria equations can be manipulated to yield the failure load as a function of the force applied to the model ($P_{applied}$), the energy release rate determined from the model ($G_{I\ applied}$ or $G_{II\ applied}$), and the critical energy release rates (G_{Ic} or G_{IIc}). Equations (10) through (16) show the fracture failure criteria equations rearranged to predict the failure load for mode I, mode II, mixed linear, mixed quadratic, mixed bilinear, and interactive biquadratic, respectively.

$$P_{fail} = \sqrt{\frac{G_{Ic}}{G_{I\,applied}}}\; P_{applied} \tag{10}$$

$$P_{fail} = \sqrt{\frac{G_{IIc}}{G_{II\,applied}}}\; P_{applied} \tag{11}$$

$$P_{fail} = \frac{1}{\sqrt{\dfrac{G_{Ic}G_{II\,applied} + G_{IIc}G_{I\,applied}}{G_{Ic}G_{IIc}P_{applied}^2}}} \tag{12}$$

$$P_{fail} = \frac{1}{\sqrt[4]{\dfrac{G_{Ic}^2 G_{II\,applied}^2 + G_{IIc}^2 G_{I\,applied}^2}{G_{Ic}^2 G_{IIc}^2 P_{applied}^4}}} \tag{13}$$

<div align="center">Bilinear:</div>

$$P_{fail} = \sqrt{\frac{G_{Ic}}{G_{I_{applied}} - \xi\left(G_{II_{applied}}\right)}}\, P_{applied} \tag{14}$$

$$P_{fail} = \sqrt{\frac{G_{IIc}}{G_{II_{applied}} - \dfrac{1}{\zeta}\left(G_{I_{applied}}\right)}}\, P_{applied} \tag{15}$$

<div align="center">Interactive Biquadratic:</div>

$$P_{fail} = \sqrt[4]{\frac{1}{\dfrac{G_{I_{applied}}^2}{G_{Ic}^2} + \dfrac{m\, G_{I_{applied}}\, G_{II_{applied}}}{G_{Ic}\, G_{IIc}} + \dfrac{G_{II_{applied}}^2}{G_{IIc}^2}}} \tag{16}$$

All criteria were calculated for each of the modeling cases explored in this research. A complete analysis to determine which of these failure criteria most accurately model the mechanics within a scarf joint was conducted. The results are discussed in the following sections.

3.   Bilinear and Interactive Biquadratic Criteria Details

The two less common failure criteria used deserve special comment. Test cases which produce answers with a small amount of variation across all the geometries are prime candidates for the bilinear and interactive biquadratic criteria. In these cases, in order to most closely approximate the existing data points, the bias of the criterion can be adjusted up and down by changing the value of the variables ζ, ξ, and m. This way error of the entire case is reduced while allowing for more accurate future predictions.

a.   Bilinear Criterion

When there are indications that a change in the failure mechanism may take place, so that one might expect different failure criteria to hold true in different regions of the mixed-mode diagram, the bilinear criterion may be applied. This criterion can be tuned to match experimental data by changing the slope of the two linear

components, ζ and ξ. The difficultly with this criteria is that the slope of either of the two legs can be adjusted to match the data. Without data that clearly defines the point where there is a change in failure mechanism, it is impossible to tell which of the lines should pass through the data, and where the intersection of these lines should be.
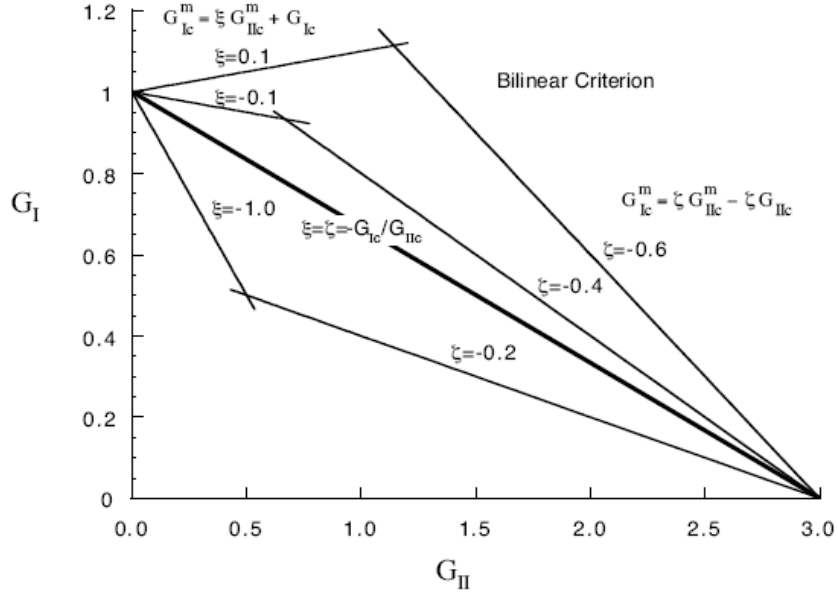
Figure 3.   Mixed-mode fracture toughness diagram for the bilinear criterion (Eq. 7 & 8) (from Ref [9])

b.   *Interactive Biquadratic Criterion*

The interactive biquadratic criterion is adjusted through the variable "m." When m is set to equal zero, the reduced equation is the same as the standard mixed quadratic criteria (see Equation 6). By varying the sign and magnitude of m, the amount of interaction between mode I and mode II can be controlled. It will be shown that this technique yielded the most accurate failure predictions.

In the compression models, it was observed that the assumed initial crack was over-closing. It was closing beyond the point where, in reality, the two crack faces would touch (see Figure 4). From this observation, it was concluded that there was no Mode I stresses at the crack tip, so G_I was set equal to zero in the failure prediction calculations, described above.   With $G_I = 0$, the Mode I terms reduce out of the failure

criteria equations for linear and quadratic mixed modes, as well as for interactive biquadratic. Compression predictions, therefore, become simply based on Mode II.
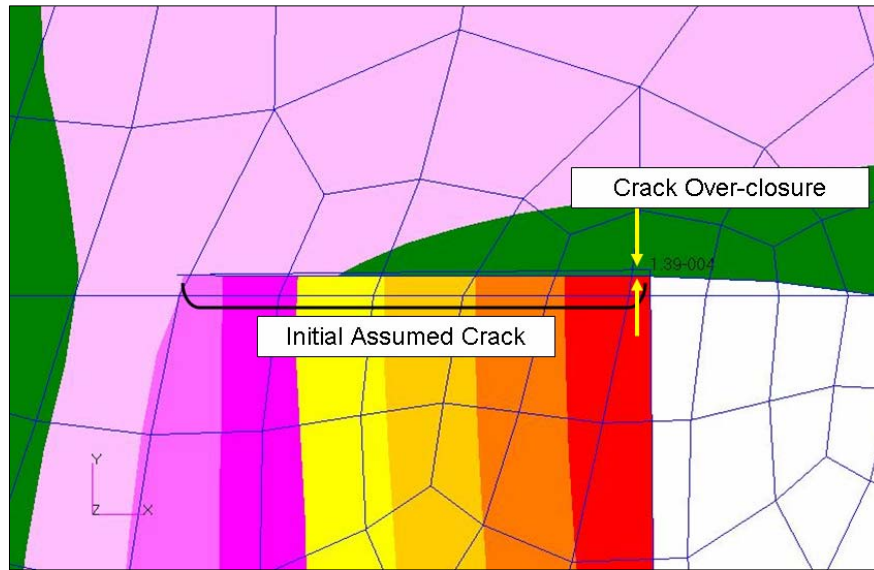
Figure 4.   Crack Over-closure in Compression. Figure is a section of a local model under compression. Color represents displacement in the Y-direction.

B.   FINITE ELEMENT MODELING TECHNIQUES

1.   Global/Local/Elemental Modeling

The global/local/elemental model technique is based on interaction between different levels of analysis. Separate scales for each model allow details to be more refined surrounding key failure areas. More importantly, the size of the mesh used to divide the model into elements can be appropriate to the geometric dimensions of the model. In this way, extreme detail in important areas can be achieved, without the burden of unnecessarily large numbers of elements.

a.   Model Geometry

In order to validate the modeled results with existing experimental data, the specimen geometry used for this research is same as was used in the NSWCCD test program. The test specimens consisted of solid laminate plates with a scarfed section in the center. The thickness of the plate and the scarf taper ratio were varied, and all four variants were modeled. The test specimens were constructed using a [0/±45/90], non-

symmetric, stack of 24 oz/yd^2 E-glass woven-roving and Dow Derakane 510A vinyl ester resin matrix. The specimens were 9.525 cm wide and had a tested gage length of 22.86 cm. The properties of the four specimens modeled and tested are shown in Table 1.

Table 1.   Scarf Configuration Matrix

Configuration ID	Thickness (t)	Taper ratio (L/t)
	cm	
Scarf 1	0.968	4:1
Scarf 2	1.463	4:1
Scarf 3	0.968	8:1
Scarf 4	1.463	8:1

All models were built within MSC.PATRAN and analyzed using MSC.NASTRAN. [10] The models built are all two-dimensional, where the specimen thickness is accounted for by multiplying the calculated resulting force by the thickness (9.525 cm). Quad4 elements were used in most cases. The only exception being when modeling the assumed crack within a resin layer, because the resin layer was a narrow triangular region, therefore Tri3 elements fit best.

b.   *Global Model*

The first step was to create a global model according to the overall test specimen dimensions. The upper and lower ply terminations were included, and were located so that the center of the scarf was at the center of the specimen. These positions varied based on the specimen thickness and the scarf ratio.
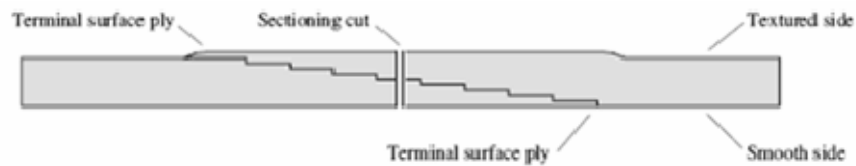
Figure 5.   Global model terminology. (from Ref [11])

Boundary conditions were determined in order to most closely reproduce the conditions the specimens underwent in experimental testing. The global model was fixed at one end in both displacement and rotation.   The other end was displaced

±0.02413 cm axially, but not allowed to displace or rotate in any other axis. In order to determine the overall force applied, the resultant nodal forces along the displaced edge were summed. This was checked at the fixed edge as well to ensure that the sum of the forces acting on the model equaled zero. This applied load was then entered into the crack closure equations discussed above, and compared with the energy release rates to determine the failure load.

The mesh within the global model was seeded so that nodes were created in the interior of the model in defined positions surrounding the area of interest (the lower ply termination). This was an important step, because the displacements of these nodes in the interior of the global model became the boundary conditions of the local model.

c. *Locating the Local Model*

In the case of the step/overlap type of scarf joint (see Figure 1), extensive testing by NSWCCD has shown that, under tension, delamination of the fiber plies always initiates failure. The areas most prone to delamination are the ply terminations at the outer surfaces. (See Figure 5) More specifically, it has been shown that the outer surface of the laminate that was against the mold during fabrication (i.e., the "smooth side") is the most likely to fail first. After initiation, this condition either progresses through the entire joint, or it precipitates premature net tensile failure vertically through the specimen.[12] The global modeling that was accomplished for this research agrees with the experimental results, showing the highest stress levels in the scarf joint at the lower ply termination. The second highest stress in the global model is at the upper ply termination. The geometry at both of these locations is essentially a corner that serves to concentrate stresses. With the knowledge that the lower terminal surface ply is the location most susceptible to delamination precipitating failure, the detail local models were focused around the lower ply termination.
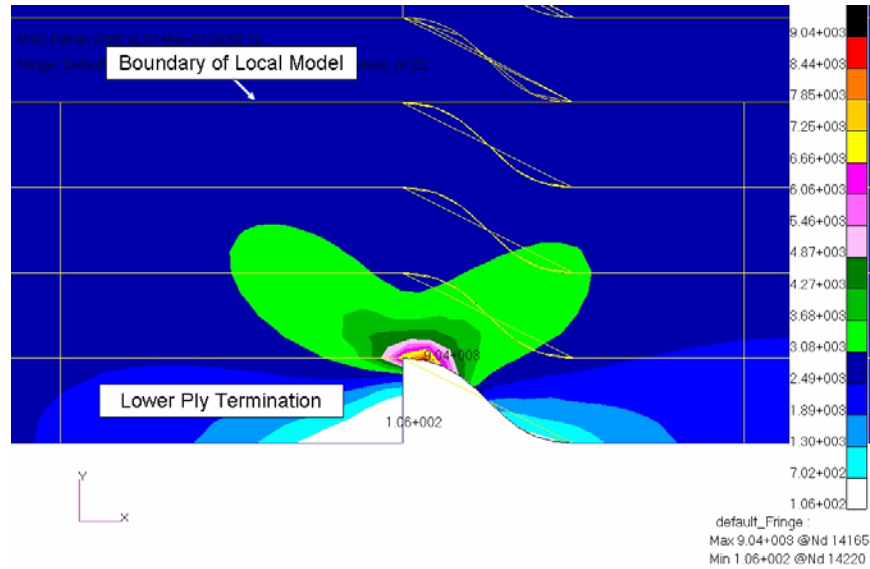
Figure 6.   The section of an isotropic global model surrounding the lower ply
termination. The stress concentration caused by the notch is evident.
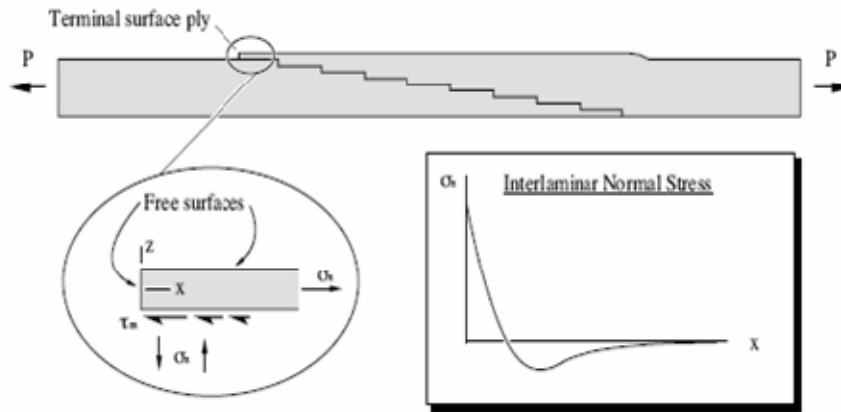
Figure 7.   Eccentric loading at the terminal plies create an internal moment which
initiates delamination. The same is true at both the upper and lower terminal
surface plies. (from Ref [13]) For example see [14].

d.   Constructing the Local Model

The dimensions of the lower model were designed to be large enough so
that stress field caused by the ply termination and the assumed crack would not affect the
boundary conditions. Because the model was assumed to be linear elastic, Saint-Venant's

principle was applicable. The height of the local model is four-ply thicknesses (4*0.06096 cm), and the length is twice the height. This size places the boundary conditions more than seven times the length of the flaw away from the area of high stress. This is more than enough distance to eliminate the interaction. [15]

The boundary conditions of the local model were taken directly from the global model. The displacements taken from the nodes seeded within the global model were entered at the edges of the local model. This reproduced the loading which the local section of the specimen was under when the entire specimen was displaced 0.02413 cm.

The assumed crack which was not modeled in the global model was included in local model. A crack length of 0.0254 cm was modeled. As discussed earlier, this length was based on the results from NSWCCD testing. This crack was constructed in the model by placing two nodes in the same location, and associating one node with the surface above it and the other with the surface below it, without connecting them with each other. Without being tied together, they were allowed to separate as the model was deformed. This separation created the crack opening measurement (Δu), or the distance between the two sides of the crack, which was then used in the CC calculations. The only difficulty with this technique was when modeling compression loads, which will be discussed later. For every case, the local model was run two times. The second time the nodes at the tip of the crack were untied, allowing crack to grow by the length of one element. This increment of crack growth (Δa) was also included in the CC calculation.

In order to model the delamination which causes failure, the crack was located between the first and second plies, in the area most prone to delamination. There is the highest stress concentration in this area because the geometry of one ply overlaying the other (terminating) ply creates a notch at this point. (see Figure 6) Any matrix material that would be filling the notch formed by the ply overlap is assumed to lend no structural support in tension and therefore is not modeled.
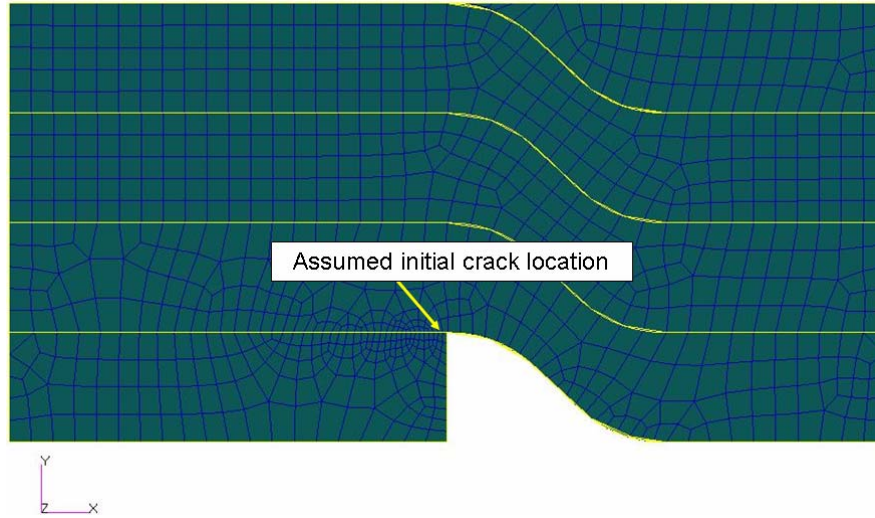
Figure 8.   Local isotropic model surrounding the lower ply termination. The notch caused by overlapping the plies concentrates stress. Note the refined mesh in vicinity of the assumed initial crack location.

Two different variants of the crack, both at the same length, were tested. One was a horizontal crack that assumed a crack path along the interface between the plies (following the yellow line in Figure 8). The other was a tapered crack with a slope matching the taper ratio of the scarf joint. Without using a tapered crack there is no way to account for differing scarf taper ratios because the size of the local model is much smaller than the geometry of the joint. This is discussed in further detail in section 3 of this chapter.

The key results taken from the local model were the crack opening measurement (Δu), the increment of crack growth (Δa), and the displacements of the element at the crack tip (which provided the boundary conditions for the elemental model). The only missing piece of information was the force at the crack tip holding the material together; not allowing the crack was allowed to grow.

e.   *Elemental Model*

For this research the modeling technique was taken one step farther and an elemental model was built which ultimately yielded the forces at the crack tip. The displacements of the element at the crack tip were taken from the local model used to

build a third FE model. This model only consisted of only one element, which was given the material properties of the section in the local model that the crack was being modeled within. One of the nodes at a corner of this elemental model undergoes the forces at the exact crack tip. Taking the forces experienced at that node, along with crack opening measurement (Δu), and the increment of crack growth (Δa), the applied energy release rates ($G_{I\ applied}$ or $G_{II\ applied}$) could be calculated. That result could then be compared with the critical ERRs (G_{Ic} or G_{IIc}) and the total load applied on the global model, in order to predict the failure load.

2 Three Standard Modeling Cases

One goal of this research was to determine the amount of detail that should be included in a FE model of a composite scarf joint. For this reason, three different modeling cases were tested with every variation of geometry. The cases each included an increasing amount of detail. The simplest case was an isotropic model. The next was still isotropic but included a resin layer interface at the secondary bond. The third modeling case was orthotropic with the individual properties of the plies modeled.

a. *Isotropic*

The isotropic model used the same material properties throughout the entire laminate. There was no specification of the orientation of individual plies. Elastic and fracture properties used to analyze this material system are shown in Table 2. [16]

Table 2.   E-glass Laminate Properties (from Ref [16])

E_{xt}	2.5	Msi
E_{yt}	2.5	Msi
E_z	1.15	Msi
G_{xy}	0.96	Msi
G_{xz}	0.42	Msi
G_{yz}	0.42	Msi
ν_{xy}	0.3	
ν_{xz}	0.24	
ν_{yz}	0.24	
$G_{Ic} \pm$ STD	1.75 ± 0.32	in*lb/in^2
$G_{IIc} \pm$ STD	7.31 ± 2.08	in*lb/in2
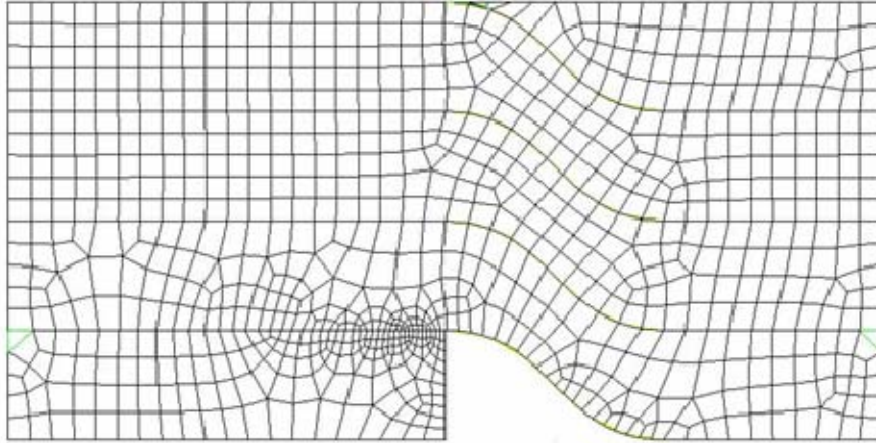
Figure 9.   Isotropic Local Model

b.   *Isotropic with Resin Layer*

The second standard modeling case used the same laminate properties as the isotropic case; however a resin interface was included in the model. This interface represents the secondary bond at the edge ply in the area of the crack tip. It was only modeled between the first and second fiber ply, immediately surrounding the assumed crack. (see Figure 10). The material properties used for the resin interface layer are listed in Table 3.

Table 3.   Neat Resin Properties (from Ref [4])

E	1.21	Msi
G	0.47	Msi
ν	0.28	
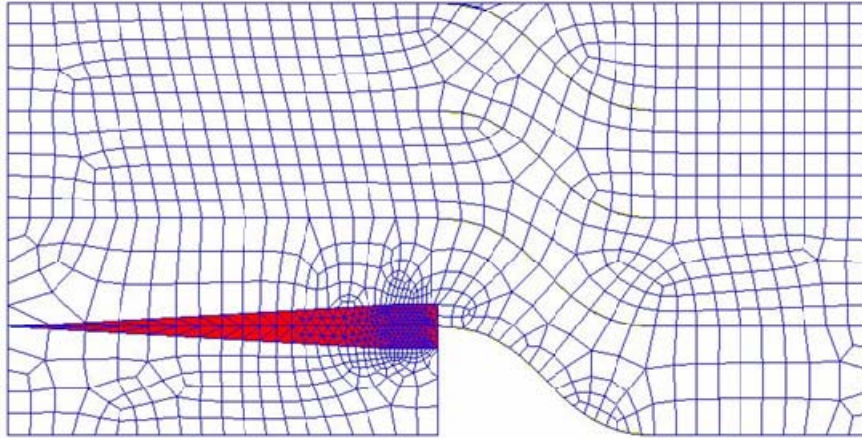
Figure 10.   Local isotropic model with the resin interface layer of 40% ply-thickness modeled (in red).

To determine the thickness of the resin layer for the model, cross-sectional images of actual scarf joints were examined and the interface thicknesses at key locations were measured. The images below clearly show a variable thickness over the length of the joint with interface thickness between 10% and 40% of one ply thickness. (See Figure 11)
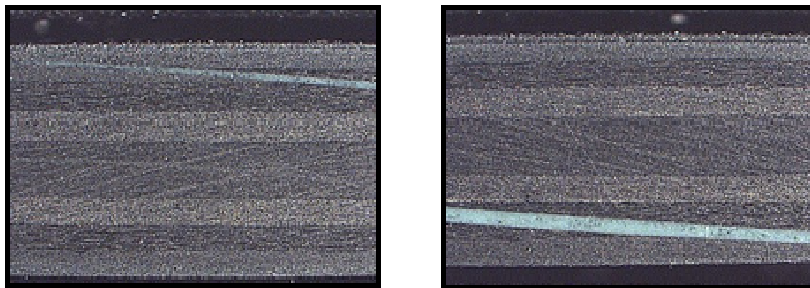
Figure 11.   Cross-sectional photo showing the variation in bond line thickness within the scarf joint. (from Ref [17])

Two models were made, one with an interface thickness at the crack that was 40% of one ply and the second with a resin layer that was only 10% of a single ply. The two models produced the same result within 2% of each other. It was concluded that the thickness of the modeled resin layer did not have a significant influence on the results. For all other model cases the 40% thickness was applied.

In order to prevent applying the boundary conditions to elements with different material properties, the resin interface could not be modeled all the way to the edge of the local model. Instead the resin layer was modeled with its 40% thickness at the edge where the crack initiates, tapering down to a point at the outer boundary. This resulted in a triangular section, and was meshed using Tri3 elements. (See Figure 10)

c.   Orthotropic

The most detailed model was the orthotropic model where each individual fiber ply was modeled separately and was given its own material properties. The local orthotropic model also included the triangular resin interface layer described above.
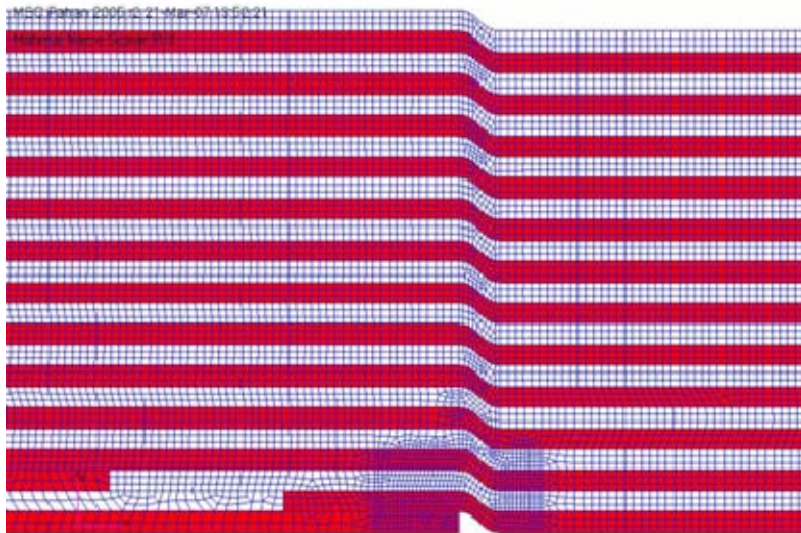
Figure 12.   Section of a global isotropic model. Detail of area around lower ply termination. Red indicates a 0/90° ply, white indicates a ±45° ply. Note the refined mesh surrounding the lower ply termination.

(1)   Individual Lamina Properties.   The specimens tested were constructed using a [0/±45/90]NS stacking sequence. Individual lamina properties for the 24 oz/yd2 E-glass are given in Table 4. [18]

Table 4.   Lamina Properties Used for Orthotropic Model

E_{xt}	3.1	Msi
E_{yt}	3.1	Msi
E_z	1.15	Msi
G_{xy}	0.56	Msi
G_{xz}	0.42	Msi
G_{yz}	0.42	Msi
v_{xy}	0.15	
v_{xz}	0.24	
v_{yz}	0.24	
$G_{Ic} \pm STD$	1.75 ± 0.32	in*lb/in^2
$G_{IIc} \pm STD$	7.31 ± 2.08	in*lb/in2

        (2)   Determining Oriented Ply Material Properties.   In order to determine the properties of the lamina that are stacked at 45°, the following equations (17 through 21) were applied to transform the properties from those of a 90° ply to those for a ±45° ply. [19] ($n = \sin\theta$, $m = \cos\theta$)

$$\frac{1}{E_x} = \frac{m^4}{E_1} + \frac{n^4}{E_2} + \left(\frac{1}{G_6} - \frac{2v_1}{E_1}\right)m^2n^2 \tag{17}$$

$$\frac{1}{E_y} = \frac{n^4}{E_1} + \frac{m^4}{E_2} + \left(\frac{1}{G_6} - \frac{2v_1}{E_1}\right)m^2n^2 \tag{18}$$

$$v_x = E_x\left[\frac{v_1}{E_1} - \left(\frac{1}{E_1} + \frac{2v_1}{E_1} + \frac{1}{E_2} - \frac{1}{G_6}\right)m^2n^2\right] \tag{19}$$

$$v_y = E_y\left[\frac{v_2}{E_2} - \left(\frac{1}{E_1} + \frac{2v_1}{E_1} + \frac{1}{E_2} - \frac{1}{G_6}\right)m^2n^2\right] \tag{20}$$

$$\frac{1}{G_s} = \frac{1}{G_6} + 4m^2n^2\left(\frac{1 + v_1}{E_1} + \frac{1 + v_2}{E_2} - \frac{1}{G_6}\right) \tag{21}$$

3. Two Initial Crack Modeling Techniques

Research by NSWCCD [20] suggests two methods of modeling the assumed initial crack. The crack can either be horizontal, following the stepped contour of the individual ply drops, or it can be tapered to attempt to capture the effect of the scarfed taper angle. Both techniques showed strengths in modeling different aspects of the fracture mechanics, so both were included in this research. As stated previously, all initial cracks, whether stepped or tapered, were 0.0254 cm in length.

a. Stepped Crack

The stepped crack was the most simple to model because it only required extending a line from the corner of the first ply termination, in the direction of the experimentally observed delamination. It was necessary to mesh this area with a node separation of approximately 0.00254 cm so that the area of interest would have the necessary resolution.

b. Tapered Crack

In order to follow the anticipated path that a crack might follow between ply drops, it makes sense to model the crack horizontally. However, because the crack length is much less than one step length, there is no geometric difference in the local model due to the taper ratio of the scarf. The only difference is in the boundary condition displacements, due to the lower ply termination being located in slightly different locations on the respective global models. The advantage of the tapered crack concept is that it includes the scarf taper ratio in the local model. A disadvantage is that it does not necessarily model the actual mechanics within the joint. A growing crack would be stopped or deflected when it reached the boundary between the fiber and the resin if it actually grew in the direction of the taper.
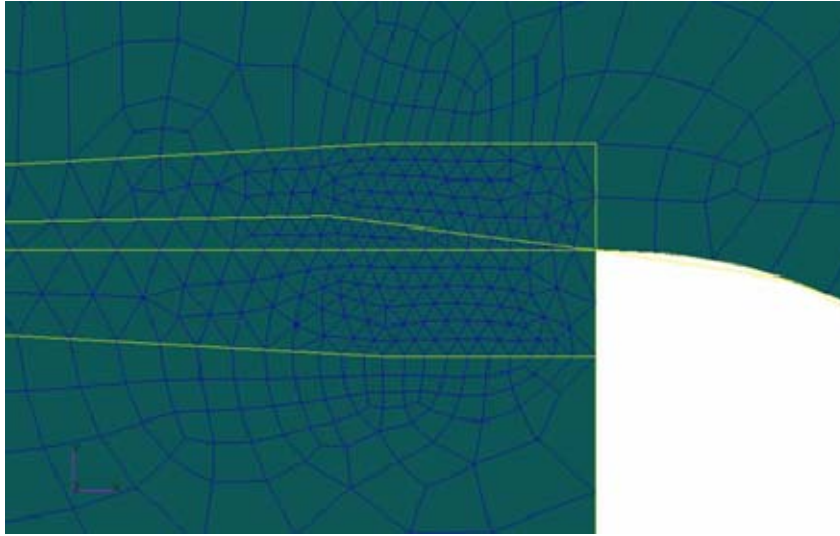
Figure 13.   Tapered crack path modeled within the resin layer. Model is for an 8:1 scarf taper ratio.

The tapered crack model was constructed by extending a line from the same point where the stepped crack began (the corner of the first ply termination) into the interior of the joint, and upward, with a slope matching the scarf taper ratio (See Figure 13). A comparison of the capabilities of these two initial crack modeling techniques in predicting failure is made in the next chapter.

One important note, output from the FE models is given in terms of the x and y axes. In order to employ the CC technique, the crack tip forces and the crack opening displacements must be in terms that are normal and tangential to the direction of crack growth. Therefore, for tapered cracks, the coordinate axes must be translated to match the crack slope.

III.   FEM PREDICTED TENSILE FAILURE LOADS

To satisfy the goal of this research and develop a finite element modeling technique which accurately predicts failure in a wide variety of scarf joints, multiple modeling cases were run and the results compared with the experimental data. As stated earlier, there were four variations of the scarf joint geometry that were used for modeling. The first variation was in thickness. One set of joints was for 16 plies of 24 oz-glass, giving a total specimen thickness of 0.968 cm. The other set was for 24 plies, with a total thickness of 1.463 cm. For each thickness, the second variation was in the scarf taper ratio (L/t). The two taper ratios studied were 4:1 and 8:1, one for each thickness, yielding a total of four different geometries to be modeled.

The three standard modeling techniques (isotropic, isotropic with an interface, and orthotropic) as well as the two initial crack modeling techniques (stepped and tapered) were employed using the global/local/elemental process for each of the four geometries. Comparison of the model results with the experimental data, show what techniques have the best correlation for specific cases, and what technique works best overall.

In addition to testing modeling techniques, it was also important to consider which fracture failure criteria most closely approximated the delamination mechanics within the joint. The criteria that were considered most closely for tension failure were mixed linear, mixed quadratic, and interactive biquadratic. Instead of picking the specific failure criterion, and model type, that gave the best result for each individual geometry, the goal was to find a combination that gave the best results over all the geometries tested.

A.   EXPERIMENTAL DATA FOR COMPARISON

The results from experimental testing conducted by the Naval Surface Warfare Center, Carderock Division, were used to compare and validate the FE models. The scarf specimens tested had the same dimensions and properties as the models. The specimens were all axially loaded in tension and compression using constant displacement to ultimate failure. [21]

Table 5.   Summary of Experimental Tensile Test Results (kN)

	Scarf 1	Scarf 2	Scarf 3	Scarf 4
	0.968, 4:1	1.463, 4:1	0.968, 8:1	1.463, 8:1
	115.7	151.2	146.8	240.2
	151.2	146.8	160.1	235.8
	146.8	186.8	142.3	204.6
	97.9	169.0	173.5	249.1
	89.0	155.7	213.5	275.8
	84.5	160.1	155.7	244.7
	111.2	164.6	146.8	253.5
	129.0	146.8	173.5	253.5
	137.9	173.5	177.9	271.3
	133.4	115.7	155.7	218.0
			146.8	
			142.3	
			164.6	
			146.8	
avg	119.7	157.0	160.6	244.7
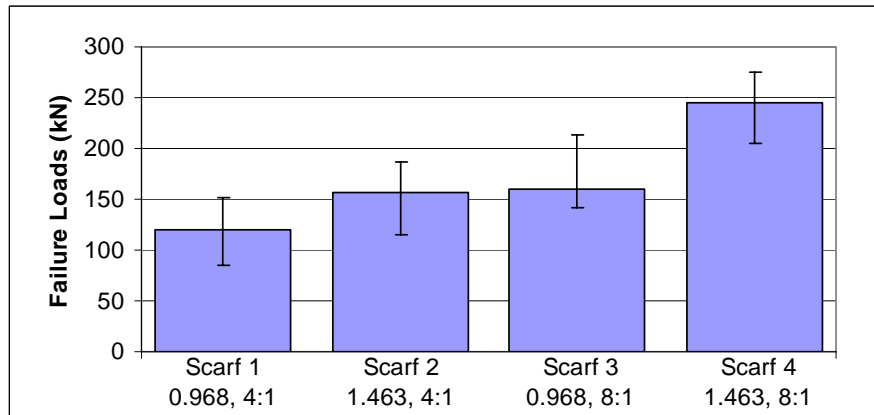
Figure 14.   Experimentally Determined Tensile Failure Loads

B.   FAILURE LOAD PREDICTION FOR EACH STANDARD MODELING CASE

1.   Stepped Model Load Predictions

Under tension, the stepped crack model was run with three variations: isotropic, isotropic with resin interface layer modeled, and orthotropic. The ERR technique presented in section II.A.1 were used to predict failure loads based on the criteria

discussed in section II.A.2. Tables 6, 7, and 8 and Figures 15, 16, and 17 show failure load predictions for the three model variations.

a.   *Isotropic Model*

In the isotropic model, the mixed linear criterion had an average magnitude error, compared to experimental data, of 32%. Mixed Quadratic had an error of 26%. Interactive Biquadratic, with the "m" variable tuned to -1.3, produced an error of 15%.   Mixed Linear and Mixed Quadratic tended to give the most conservative predictions. The stepped model is not able to accurately show the difference in scarf taper for two specimens of the same thickness (i.e.: Scarf 1/Scarf 3, or Scarf 2/Scarf 4). The only differences in the taper ratio were evident in the global models. For all criteria, the predictions overestimated the failure load for Scarf 3.

Table 6.   Scarf Tension Load Predictions – Isotropic, Stepped Model (kN)

Geometry	Mixed Linear	Mixed Quadratic	Biquadratic	Experimental
Scarf 1	86.3	95.8	112.1	119.7
Scarf 2	122.9	136.3	159.3	157.0
Scarf 3	233.7	238.0	242.3	160.6
Scarf 4	165.4	190.0	250.4	244.7

Figure 15.   Scarf Tension Load Predictions – Isotropic, Stepped Model. (M value for biquadratic = -1.3)

27

b. Isotropic Model with Resin Interface

Table 7 and Figure 16 show the failure load predictions using an isotropic, stepped crack model including a resin interface layer. Comparing criteria, the Mixed Linear had an average magnitude error of 16%, the Mixed Quadratic 17% and the Interactive Biquadratic 15% (with m tuned to 1.8). All the results show improvement over the model without a resin layer included.

Table 7. Scarf Tension Load Predictions – Isotropic, Stepped Model with Resin Interface (kN)

Geometry	Mixed Linear	Mixed Quadratic	Biquadratic	Experimental
Scarf 1	117.4	133.1	118.5	119.7
Scarf 2	176.1	199.8	177.9	157.0
Scarf 3	124.7	142.7	126.0	160.6
Scarf 4	179.6	203.8	181.5	244.7
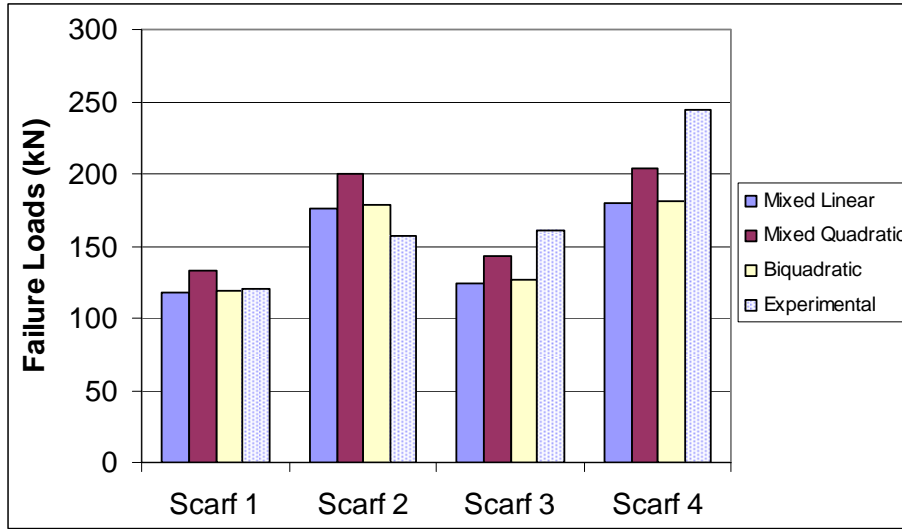
Figure 16. Scarf Tension Model – Isotropic, Stepped Model with Resin Interface

28

c. *Orthotropic Model*

The third stepped case modeled was fully orthotropic, including the material properties of each individual ply, and the resin interface layer. The properties were modified as discussed in section II.B.2 to account for the ply orientation.

The average magnitude error for all criteria was higher, indicating that including the additional detail did not improve the accuracy of the model, when using a stepped crack growth path. The errors were: Mixed Linear 18%, Mixed Quadratic 19%, and Interactive Biquadratic 18% (with m tuned to 3.0).

Table 8.   Scarf Tension Model – Orthotropic, Stepped Model (kN)

Geometry	Mixed Linear	Mixed Quadratic	Biquadratic	Experimental
Scarf 1	121.9	138.0	116.5	119.7
Scarf 2	182.5	199.8	176.2	157.0
Scarf 3	112.6	127.2	107.8	160.6
Scarf 4	189.7	217.2	180.9	244.7
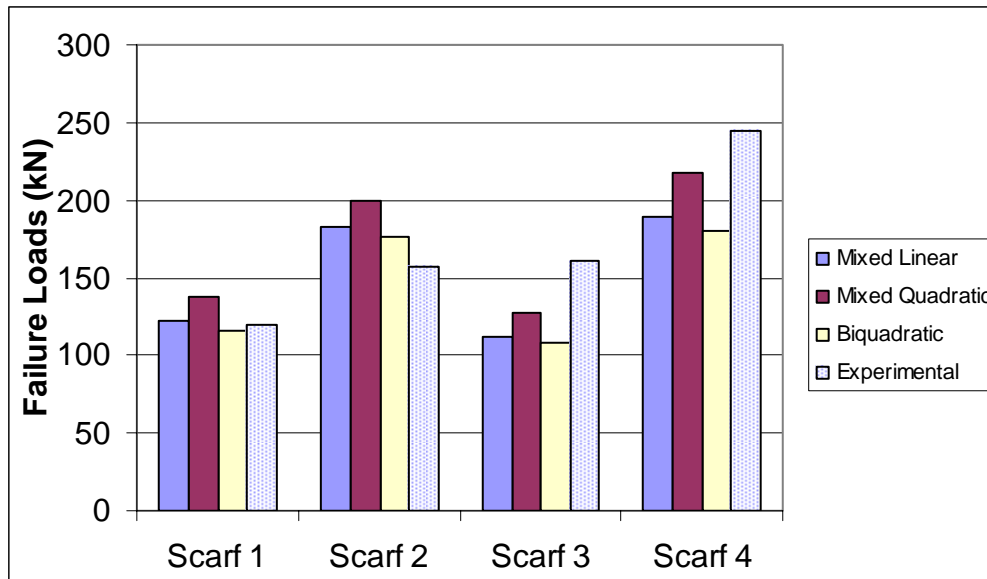
Figure 17.   Scarf Tension Model – Orthotropic, Stepped Model

d.   *Stepped Crack Model Summary*

Figure 18 shows that the isotropic model, with the resin interface layer included in the model, yielded the lowest magnitude error when the results from every specimen thickness and scarf taper ratio were averaged.

Figure 18.   Average magnitude error comparison for the three stepped model types and the three failure criteria, using a stepped crack path.

Figure 19 depicts the variance of the modeled results.   In addition to having the lowest average magnitude error, the results from the isotropic model with resin layer also had the smallest variance for the different geometries.

Figure 19.   Variance comparison for the three stepped model types and the three failure criteria, using a stepped crack path.

2. Tapered Crack Model Load Predictions

Under tension, the tapered initial assumed crack model was also run with the same three model variations: isotropic, isotropic with resin interface layer and orthotropic. Tables 9, 10 and 11 along with Figures 20, 21 and 22, below, show failure load predictions for the three model variations.

a. Isotropic Model

In the isotropic model, the Mixed Linear criterion had an average magnitude error of 40%. The Mixed Quadratic has an error of 31%. The interactive Biquadratic criterion, with an "m" value tuned to -1.8, produced an error of only 10%.

Table 9.   Scarf Tension Load Predictions – Isotropic, Tapered Model (kN)

Geometry	Mixed Linear	Mixed Quadratic	Biquadratic	Experimental
Scarf 1	80.2	93.8	137.1	119.7
Scarf 2	103.0	118.7	158.3	157.0
Scarf 3	85.0	98.0	131.6	160.6
Scarf 4	130.7	151.1	205.9	244.7
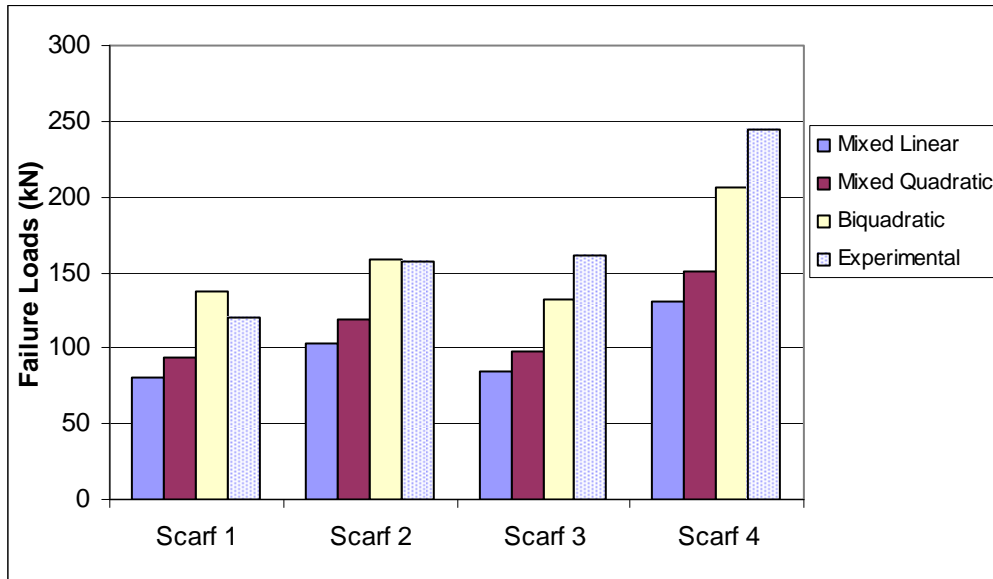
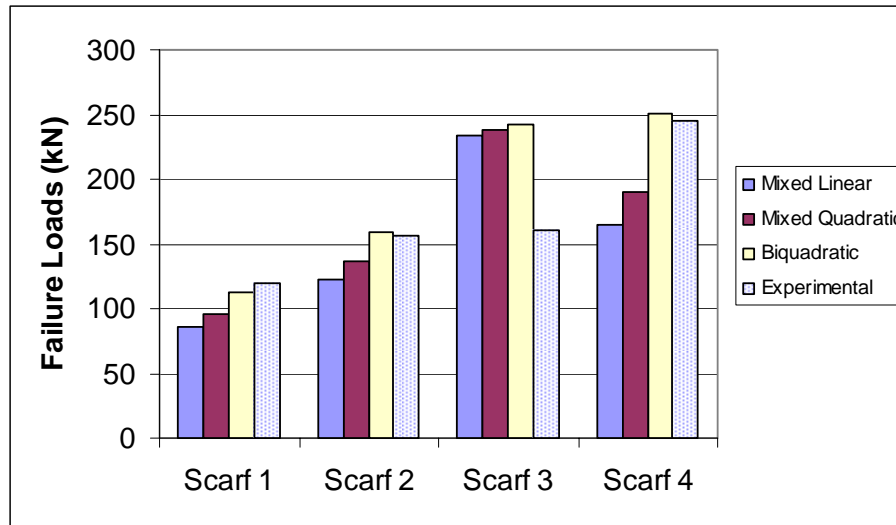Figure 20.   Scarf Tension Model – Isotropic, Tapered Model. (M value for Biquadratic = -1.8)

31

b. *Isotropic Model with Resin Interface Layer*

Table 10 and Figure 21 show the failure load predictions for an isotropic model with a resin interface, using the tapered initial crack path. The same three criteria are compared. Mixed Linear had an average magnitude error of 41%. Mixed Quadratic had an error of 31%, and Interactive Biquadratic 10% (with m tuned to -1.8).

Table 10.   Scarf Tension Model – Isotropic, Stepped Model, with Resin Interface

Geometry	Mixed Linear	Mixed Quadratic	Biquadratic	Experimental
Scarf 1	54.6	62.9	84.2	119.7
Scarf 2	93.8	108.8	150.7	157.0
Scarf 3	105.4	121.3	161.2	160.6
Scarf 4	163.5	189.2	259.0	244.7
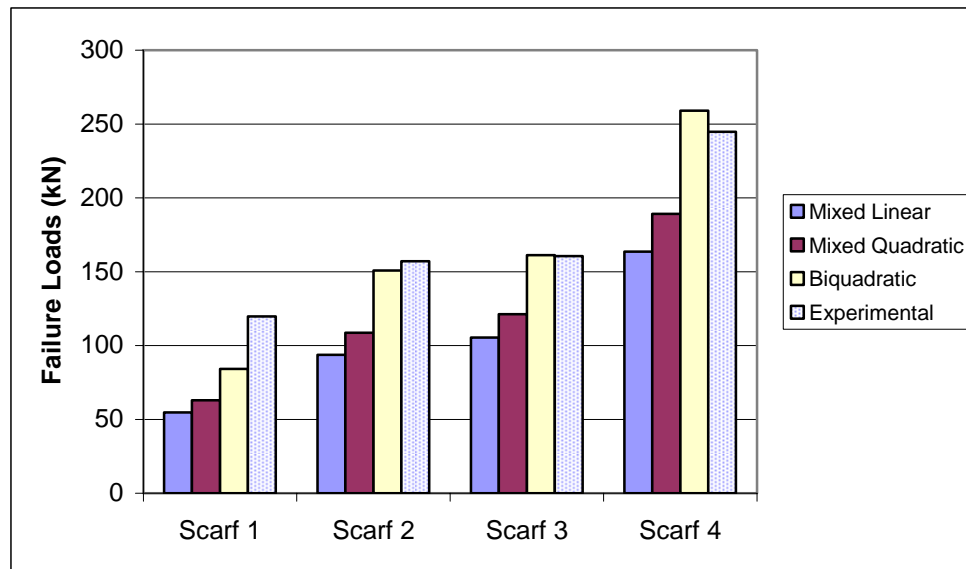
Figure 21.   Scarf Tension Model – Isotropic, Tapered Model, with Resin Interface

All cases considerably underestimated the failure loads. By tuning the interactive biquadratic criteria, the predictions were much closer to the experimental results. Notably, Scarf 2 and Scarf 3 were within 4% and <1% of the experimental results, respectively.

c. *Orthotropic Model*

The third tapered case modeled was orthotropic with a resin interface layer. The individual material properties for each ply were included in the model, modified to match the ply orientation.

The average magnitude error for each criterion was as follows: Mixed Linear 37%, Mixed Quadratic 28%, and Interactive Biquadratic 14%. The "m" value for the biquadratic was tuned to -1.8, just as it was for the tapered orthotropic and the tapered orthotropic with the interface layer.

Table 11.   Scarf Tension Model – Orthotropic, Tapered Model (kN)

Geometry	Mixed Linear	Mixed Quadratic	Biquadratic	Experimental
Scarf 1	82.2	93.6	118.6	119.7
Scarf 2	115.4	132.5	174.0	157.0
Scarf 3	86.6	97.8	119.9	160.6
Scarf 4	138.7	157.4	197.2	244.7
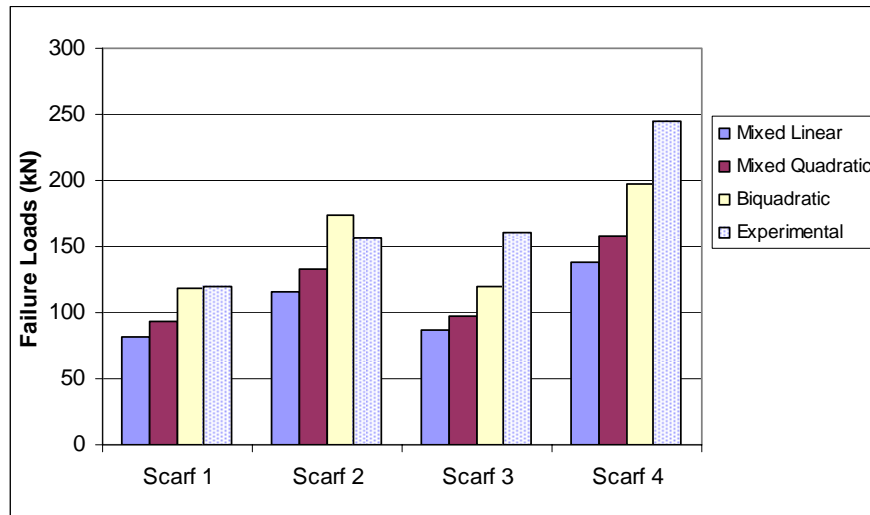
Figure 22.   Scarf Tension Model – Orthotropic, Tapered Model (M value for biquadratic = -1.8)

The orthotropic, tapered models were consistently conservative, underestimating the tensile failure load of all geometries. The only one case that overestimated the failure load was the biquadratic model for the Scarf 2 geometry.

d.   *Taper Crack Model Summary*

The tapered models consistently under-predicted the failure load for all geometric variations. Considering the traditional fracture criteria, the closest to correlating with the experimental data was the mixed quadratic. However, even this one underestimated the failure loads by anywhere between 28% and 31%. By using the Biquadratic criterion, the error range in the predictions was reduced to 10% to 14%.
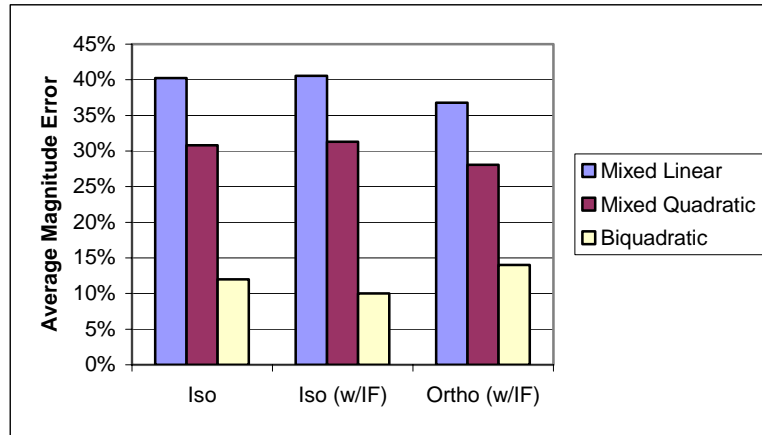
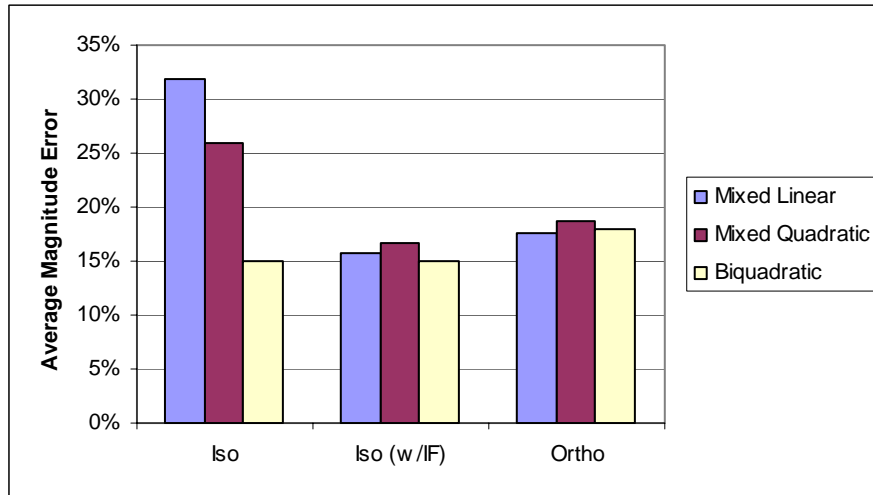Figure 23.   Average magnitude error comparison for the three stepped model types and three failure criteria, using a tapered crack path.

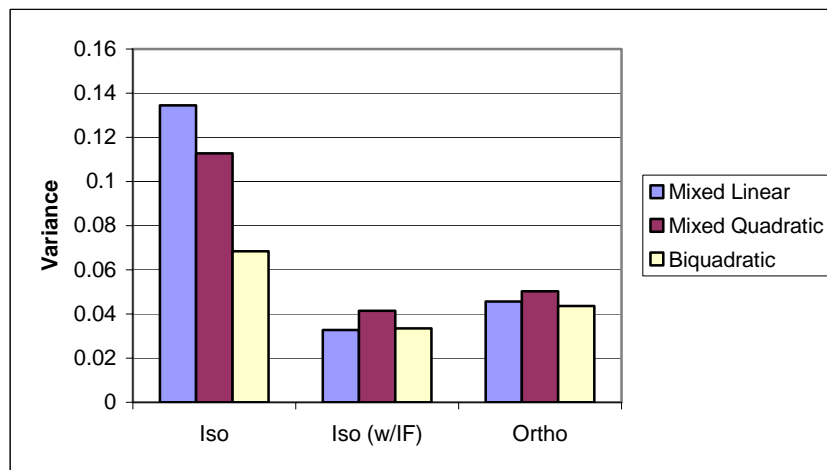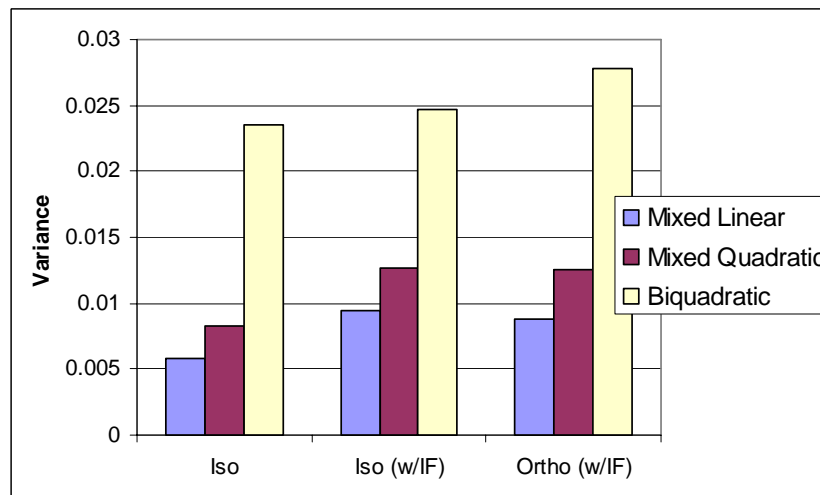Figure 24.   Variance comparison for the three stepped model types and the three failure criteria, using a tapered crack path.

Recall, the purpose of using the tapered crack path was to attempt to account for the scarf taper ratio within the scale of the local model, since the size of one step is larger than that model. The results show that the tapered models predict fairly consistent failure loads across all geometries, however the average failure load predicted is worse than most stepped models. In other words, the variance is small but the average magnitude error is large.

The best case, just as for the stepped crack models, is again the isotropic model with the resin layer. For all three model types, it was best to use the interactive biquadratic model to reduce the error to a reasonable level. Interestingly, the tuning value (m) set at -1.8 gave the lowest magnitude error and the smallest variance for all three model types with a tapered crack.

C. TENSION MODEL CONCLUSION

1. Choosing the Best Fracture Failure Criterion

Based on the summaries from the tension stepped models and the tension tapered models, figures 18 and 23, the isotropic model which includes the resin interface in the model has the lowest average magnitude error for the majority of the fracture failure criteria. Due to the ability to tune the equation to match the existing experimental data, the interactive biquadratic criterion yields the best results (Figure 25), compared with the mixed linear and mixed quadratic criteria. For some individual cases, the mixed linear criterion produced the best results, and in most cases the mixed linear was better than the mixed quadratic. However, overall, the interactive biquadratic was the best fracture failure criterion.
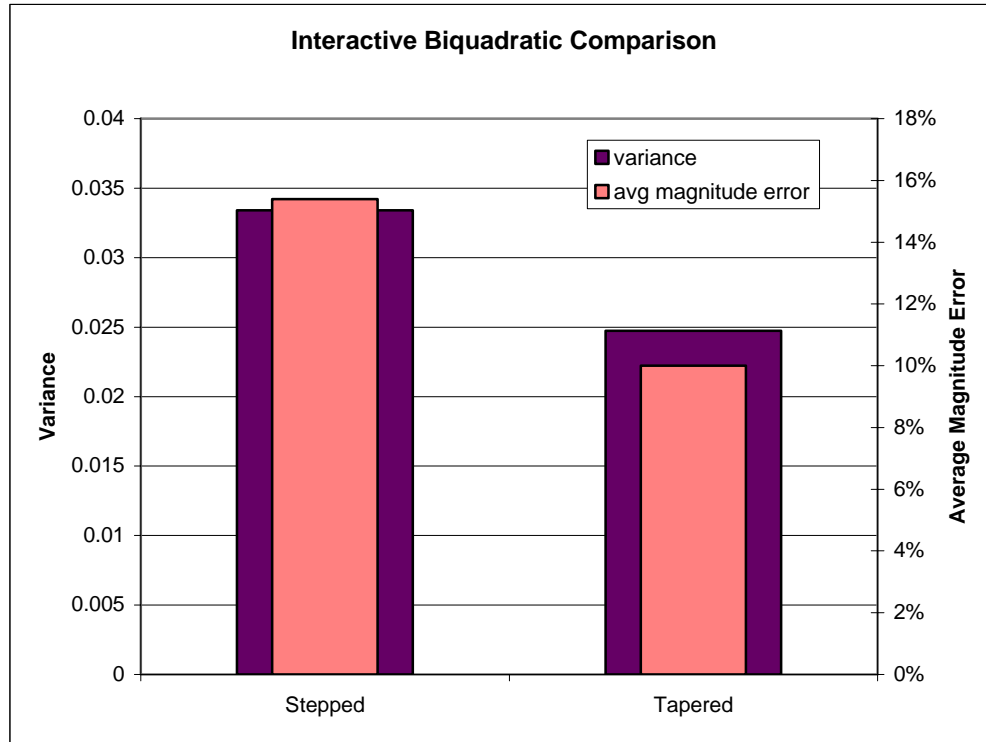
Figure 25.   Average Magnitude Error and Variance for the Stepped vs. Tapered Tensile Models Using the Interactive Biquadratic Criterion. (Note: the M value for the stepped model was tuned to 1.8 and the tapered model tuned to -1.8.)

2.   Effect of Specimen Geometry

The isotropic model, with resin interface and tapered crack path, predicted tensile failure for all geometries within 6% error, except for Scarf 1 (see Table 12). Scarf 1 had an error of nearly 30%.

Table 12.   Interactive Biquadratic Tension Failure Predictions Compared to Experimental Results – Isotropic Model with Resin Interface, Tapered Crack Path. (kN)

	Scarf 1	Scarf 2	Scarf 3	Scarf 4
	0.968, 4:1	1.463, 4:1	0.968, 8:1	1.463, 8:1
Biquadratic	84.2	150.7	161.2	259.0
Experimental	119.7	157.0	160.6	244.7
% error	29.7%	4.1%	-0.4%	-5.9%
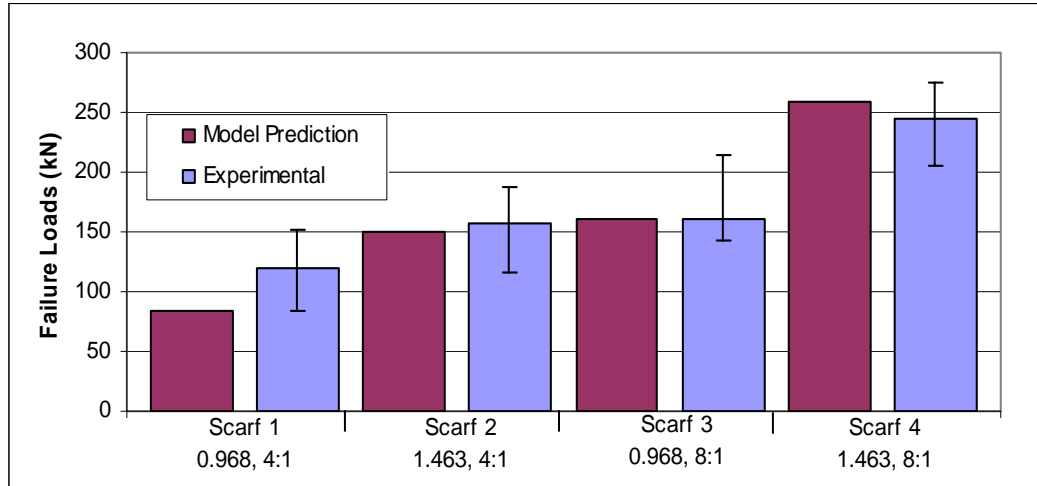
Figure 26.   Interactive Biquadratic Tension Failure Predictions Compared to
Experimental Results – Isotropic Model with Resin Interface, Tapered Crack Path

3.   Validated Model for Predicting Tensile Failure of a Scarf Joint

The best model for predicting tension failure in a composite scarf joint is the isotropic model with interface layer, using a tapered initial assumed crack path, and the Interactive Biquadratic failure criterion. The failure criterion should be tuned with an "m" value equal to -1.8 to most accurately represent the interaction between Mode I and Mode II.

THIS PAGE INTENTIONALLY LEFT BLANK

IV.   FEM PREDICTED COMPRESSION FAILURE LOADS

Just as with the tensile loads, compression failure models were also constructed and validated against NSWCCD experimental data. The same four geometric variations were modeled and tested: 0.968 cm and 1.463 cm, both with a 4:1 taper; and 0.968 cm and 1.463 cm, both with an 8:1 taper. To determine the best technique to predict compression failure, a similar analysis was performed as was done for the tensile tests.

A.   EXPERIMENTAL DATA FOR COMPARISON

The experimental data from NSWCCD for compression failure show a similar pattern as the tension failure, Figure 27. [20] The joints become stronger as the specimens increase in thickness, and also as the length of the scarf tapers increase.

Table 13.   Summary of Experimental Compression Test Results (kN). (from Ref[20])

Scarf 1	Scarf 2	Scarf 3 **	Scarf 4
0.968, 4:1	1.463, 4:1	0.968, 8:1	1.463, 8:1
-84.5	-200.2	-71.2	-306.9
-84.5	-191.3	-80.1	-293.6
-84.5	-173.5	-129.0	-302.5
-93.4	-195.7	-102.3	-275.8
-84.5	-191.3		-253.5
-80.1	-191.3		-306.9
-89.0	-204.6		-298.0
-97.9	-200.2		-311.4
-84.5	-191.3		-280.2
-89.0	-191.3		-249.1
avg -87.2	-193.1	-95.6	-287.8

**Note: The Scarf 3 configuration buckled consistently under compressive loading. Attempts to restrict the buckling were unsuccessful. After four specimens were tested the remaining samples were used for tensile testing. [20] Due to the similarities between Scarf 2 and Scarf 3 in tension testing, for validation of FE model data, the ultimate compression loads for Scarf 3 were assumed to be the same as for Scarf 2.
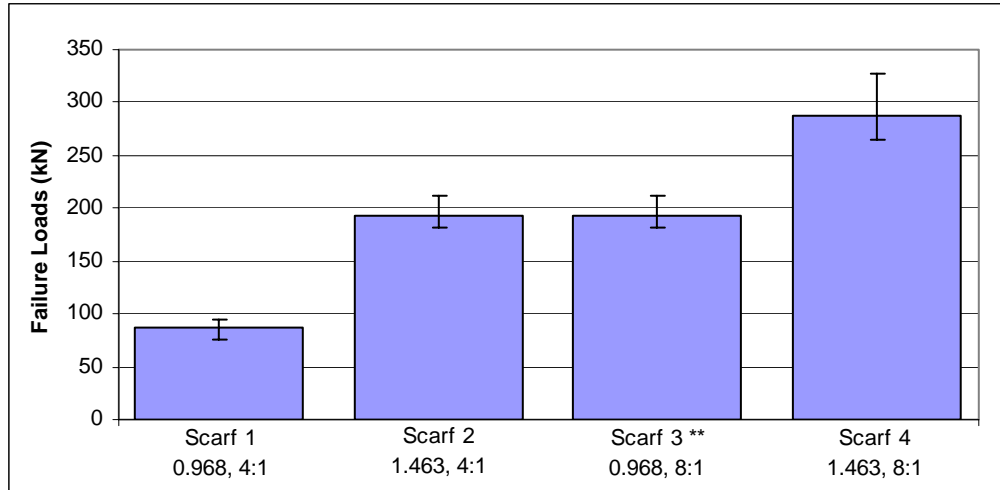
Figure 27.   Experimentally Determined Compression Failure Loads. Scarf 3 values set
equal to Scarf 2 to compensate for buckling and to allow for model validation.

B.   FAILURE LOAD PREDICTION FOR EACH INITIAL CRACK TYPE

Building off the success of the isotropic model with resin layer in the tension tests, this same model was used as the starting point for compression modeling. Using this model type, the initial assumed crack type was varied to determine the combination which best predicted compressive failure loads.

The only failure criterion considered was Interactive Biquadratic. As discussed earlier, in compression the G_I values are all equal to zero due to crack closure. Therefore, Mixed Quadratic and Interactive Biquadratic under compression reduce to be the same as Mode II. For consistency with the tension results, the Interactive Biquadratic criterion name is going to be used for all results.

1.   Stepped Initial Crack Model Load Predictions

Under compression, the stepped crack growth path model was run. Table 14 and Figure 28 show failure load predictions for the four geometric variations. The fracture criterion was not conservative, over-predicting error and shows a fairly high average magnitude error of 68%. Scarf geometry 3 and 4 are the notable exceptions, with prediction errors less than 1/3 as much as the shorter taper ratio of Scarf 1 and 2.

40

Table 14.   Scarf Compression Load Prediction – Isotropic, Stepped, w/ Resin
Interface (-kN)

Geometry	Biquadratic	Experimental
Scarf 1	224.9	87.2
Scarf 2	337.6	193.1
Scarf 3*	229.1	193.1
Scarf 4	344.3	287.8
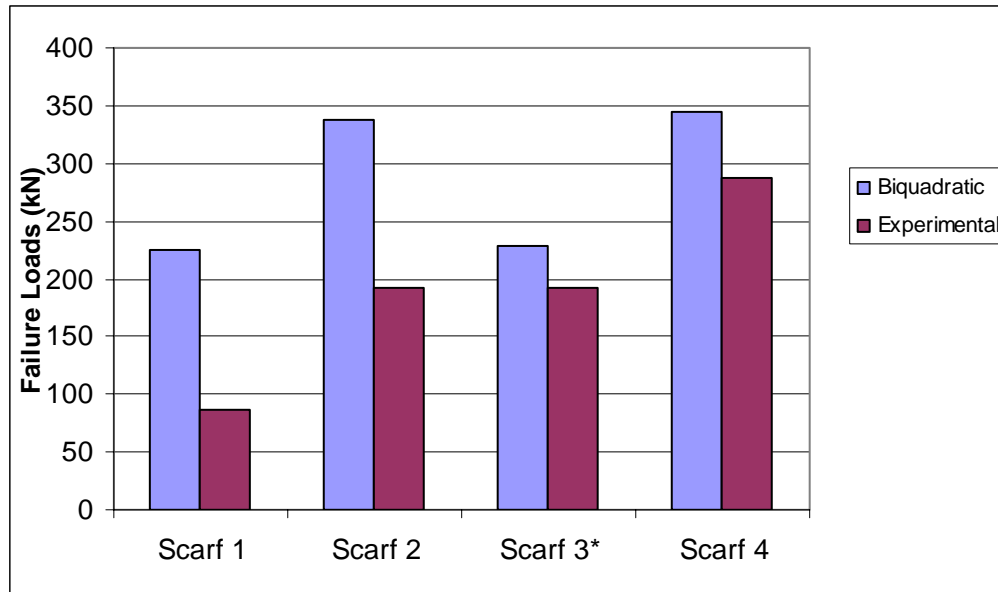
Figure 28.   Scarf Compression Load Predictions – Isotropic, Stepped, with Resin
Interface

2.   Tapered Initial Crack Model Load Predictions

The tapered crack model was much more accurate than the stepped model in predicting compression failure (see Table 15 and Figure 29). The average magnitude error was 8% for Interactive Biquadratic.

Table 15.   Scarf Compression Model Predictions – Isotropic, Tapered, with Resin
Interface (-kN)

Geometry	Biquadratic	Experimental
Scarf 1	96.9	87.2
Scarf 2	161.4	193.1
Scarf 3*	188.3	193.1
Scarf 4	284.3	287.8
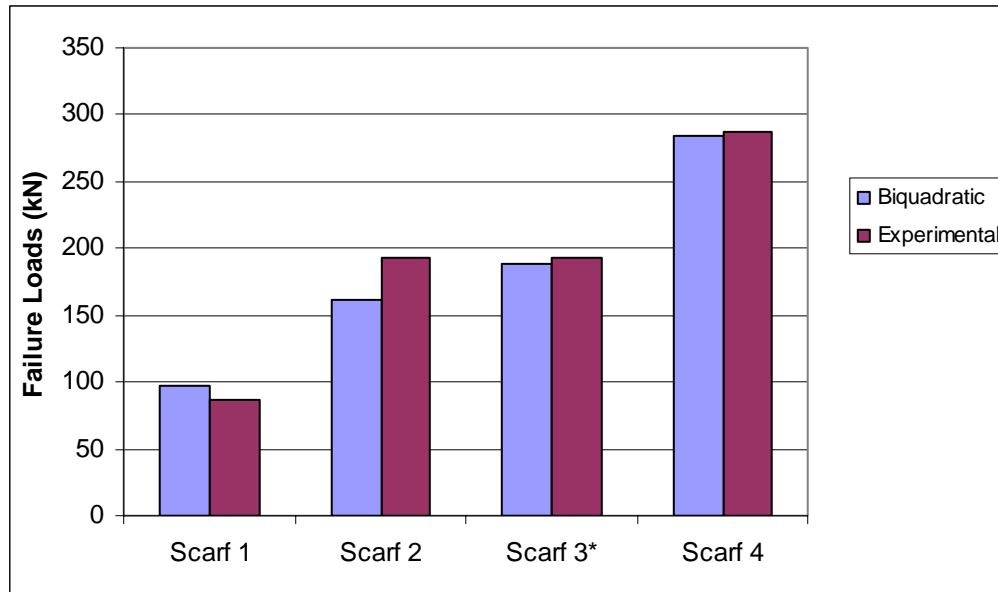
Figure 29.   Scarf Compression Model Predictions – Isotropic, Tapered, with Resin
Interface

C.   COMPRESSION MODEL CONCLUSION

1.   Choosing the Best Compression Modeling Technique

When comparing the stepped crack modeling technique with the tapered crack technique, the compression model agrees with the tension model, getting the best predictions with a tapered initial crack path. As shown in Figure 30, the average magnitude error of the tapered models was much less than the stepped models, 8% vs. 68% error. The variance of the tapered data was also much smaller, with the total error range across all four geometries being between -16% and 11%.
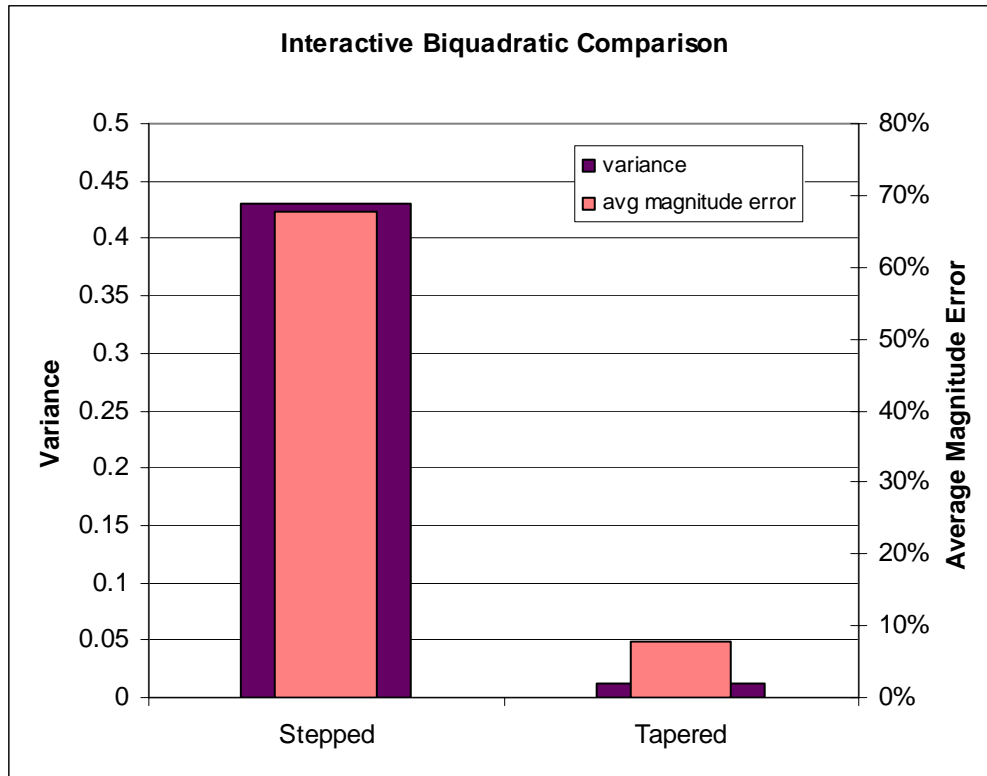
Figure 30.   Average Magnitude Error and Variance for the Stepped vs. Tapered
Compression Models Using the Interactive Biquadratic Criterion.

2.   Validated Model for Predicting Tensile Failure of a Scarf Joint

The best model for predicting compression failure in a composite scarf joint is the isotropic model with interface layer, using a tapered initial assumed crack path, and the Interactive Biquadratic failure criterion. It is important to remember the failure criterion is equal to the Mode II results for compression cases. Overall, this combination yielded accurate failure load predictions.

D.   ADDITIONAL COMPRESSION MODEL RESULTS

1.   Effect of Specimen Geometry

The geometry of the samples being modeled had a much more pronounced effect in the compression modeling, compared with the tension modeling. The thickness of the specimen was not a factor in the modeling, however the taper ratio was. The model predicted the compression failure load for both 8:1 specimens very accurately, 2.5% error

for Scarf 3 and 1.2% error for Scarf 4. The shorter, 4:1 taper, proved more difficult to predict, with errors of -11.2% and 16.4% for Scarf 1 and Scarf 2, respectively.

Table 16.   Interactive Biquadratic Compression Failure Predictions Compared to Experimental Results – Isotropic Model with Resin Interface, Tapered Crack Path. (values in -kN)

	Scarf 1	Scarf 2	Scarf 3**	Scarf 4
	0.968, 4:1	1.463, 4:1	0.968, 8:1	1.463, 8:1
Biquadratic	96.9	161.4	188.3	284.3
Experimental	87.2	193.1	193.1	287.8
% error	-11.2%	16.4%	2.5%	1.2%
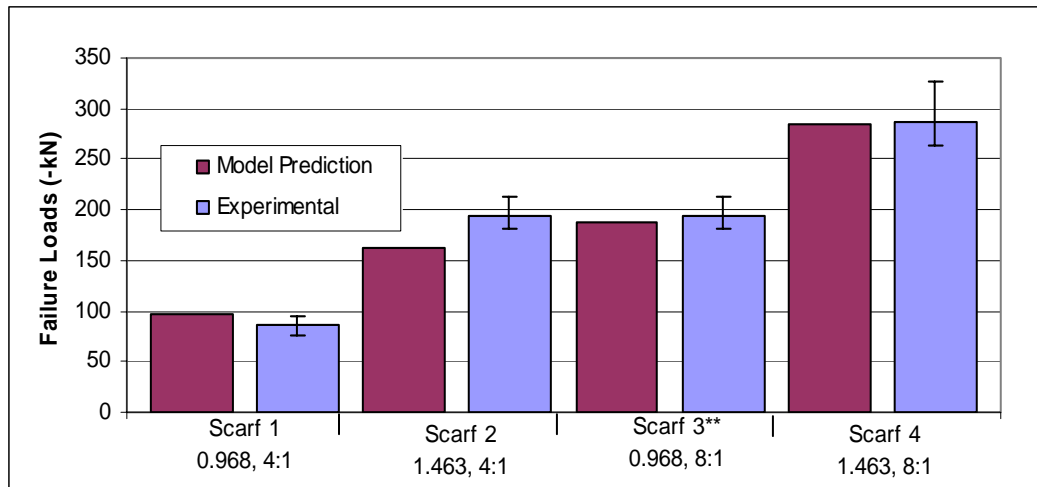
Figure 31.   Interactive Biquadratic Tension Failure Predictions Compared to Experimental Results – Isotropic Model with Resin Interface, Tapered Crack Path

2.   Out-of-Axis Force to Simulate Pre-existing Curvature

A second technique used to attempt to reproduce the failure mechanics of a scarf joint under compression was to add an external force in the transverse direction. This out-of-axis load was included to attempt to account for bending of the sample under compression. It was thought that the bending, while not leading to buckling, may still add internal stresses to the joint that should be included in the modeling. It was not necessary to include this out-of-axis load in the tension models because any curvature in

those samples would be corrected by tensioning prior to approaching failure. In the compression models, any pre-existing curvature would only be exasperated by the testing.

Out-of-axis forces of 1% and 0.5% of the total compressive load were applied to the global model at the midpoint, in both the positive-y and negative-y directions. (See Figure 32) The ERR process was then followed to determine the predicted failure load. It was thought that if the correct magnitude of out-of-axis force was applied, it would increase the accuracy of the prediction by accounting for bending occurring in the test sample. The technique did show some promise. A 0.5% load in the negative-y direction, under predicted the failure load by 48%, and a 0.5% load in the positive-y direction under predicted the failure load by 25%. Continued refinement of the out-of-axis load may lead to an accurate prediction. However, significant trial and error would be necessary to determine the proper percentage of force to apply. Ultimately, the results from the Interactive Biquadratic technique, mentioned in the previous section, predicted compression failure well, so it was not necessary to explore the out-of-axis loading technique further.
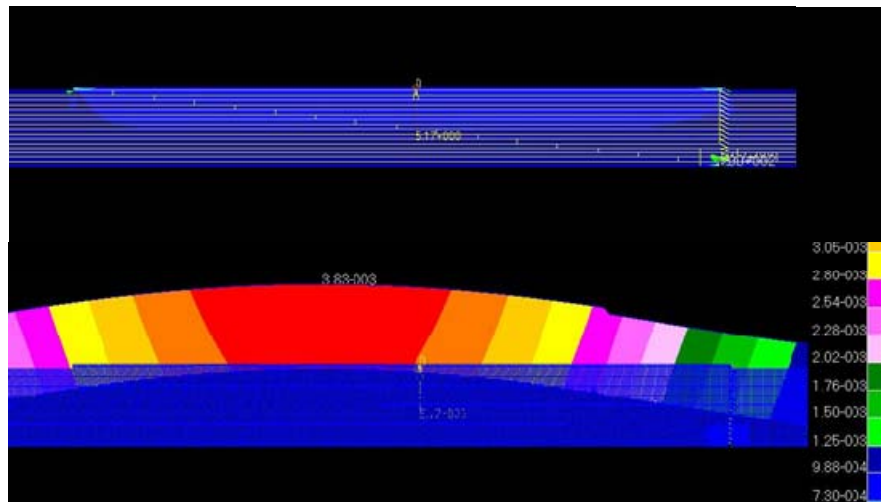
Figure 32.   Out-of-Axis Force Applied to Compression Model. The upper model shows the additional force of 0.5% the total load added in the positive Y direction in the center of the joint. The lower ply termination is in the lower right corner. The lower figure shows the displacement in the Y direction. Note the exaggeration, actual Y displacement is 0.00383".

45

3.   Location of the Local Model for Compression

It is vital to the global/local modeling technique to position the local model where there is the highest crack opening (Mode I) stress. If the assumed initial crack is not placed where the specimen begins to experience delamination, the model will not be predicting failure where the forces inside the joint are highest. Therefore the prediction will not be accurate.

Testing by NSWCCD [22], as well as Slaff [23], has revealed that scarf joints under compression often initiate delamination in the center of the joint, and not at lower ply termination. This situation implies that the compression results described in this section may be improved upon by relocating the local model to the center of the global model. This technique was pursued further and will be addressed in section V.
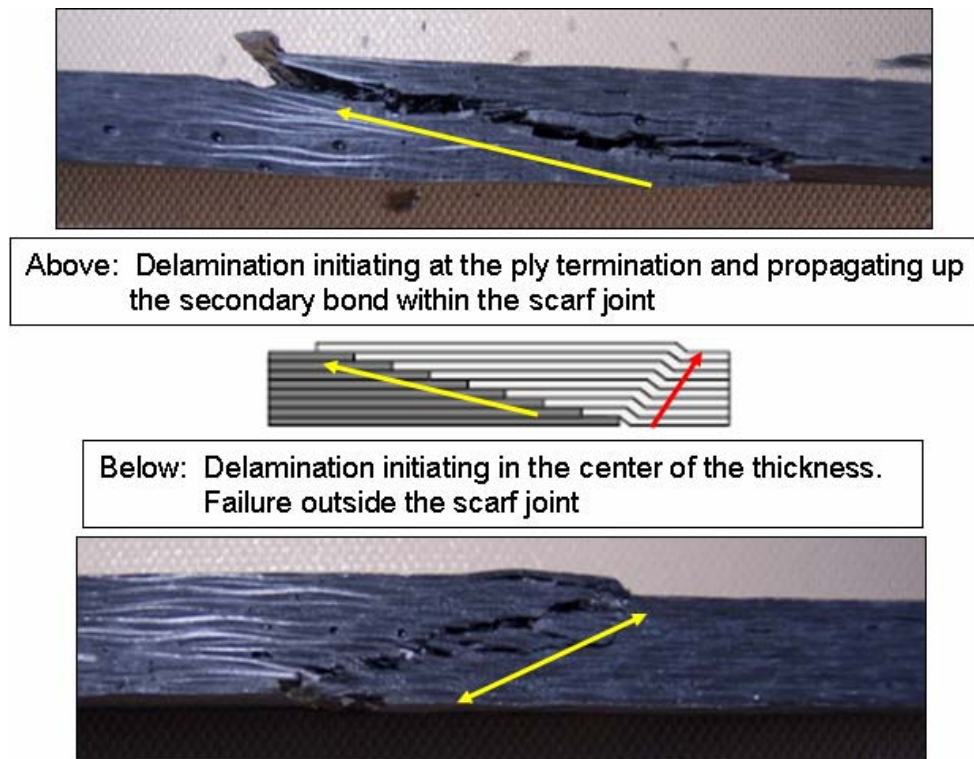
Figure 33.   Post compression test photographs showing the two observed failure types:
First, at the secondary bond, up the scarf joint. Second, away from the scarf,
initiating in the center of the thickness. (from Ref [23])

V. PREDICTED FAILURE LOADS FOR CARBON FIBER / VINYL ESTER RESIN SCARF JOINTS

The ultimate goal of this research, as stated originally, is to provide naval designers with a better understanding of the failure mechanics within a composite scarf joint. This improved understanding will allow significant cost savings in future designs by increasing the validity of results from FE models, thereby reducing the need to conduct expensive experimental testing. The next generation of warship, on the drawing board today, will employ an extensive amount of carbon fiber-based composite materials. The decision has already been made to construct the deckhouse structure of the Zumwalt class destroyer (DDG-1000) from carbon composite. Therefore, the next logical progression of this research was to apply the techniques developed in the previous sections to this new carbon fiber-based material system.

A. CARBON FIBER VS. E-GLASS

All the models described thus far were constructed using the material properties of traditional e-glass. This material was chosen because extensive experimental test results exist to validate the computer models. In comparison with e-glass, the properties of carbon fiber composites have a considerably higher tensile strength and shear modulus. For comparable structure with the same stiffness and strength, carbon construction is several times lighter. Appendix A, specifically Tables A-2 and A-3, detail the advantage of carbon fiber composites over traditional building materials. [2] Table 17 lists the carbon fiber laminate material properties used for this modeling.

Table 17.   Carbon Fiber Laminate Properties (from Ref [24])

E_{xt}	7.6	Msi
E_{xc}	8.5	Msi
E_{yt}	8.3	Msi
E_{yc}	8.3	Msi
E_z	1.3	Msi
G_{xy}	0.55	Msi
G_{xz}	0.46	Msi
G_{yz}	0.46	Msi
ν_{xy}	0.04	
ν_{xz}	0.34	
ν_{yz}	0.34	
$G_{Ic} \pm$ STD	1.75 ± 0.32	in*lb/in^2
$G_{IIc} \pm$ STD	7.31 ± 2.08	in*lb/in2

B. CARBON FIBER FINITE ELEMENT MODELS

In order to model the scarf joint with a carbon fiber-based material system, the global/local/elemental modeling process validated by the previous research with e-glass was used. The local model was isotropic, but included the resin interface layer and a tapered initial assumed crack path. In order to predict the failure load, the Interactive Biquadratic failure criterion was employed.
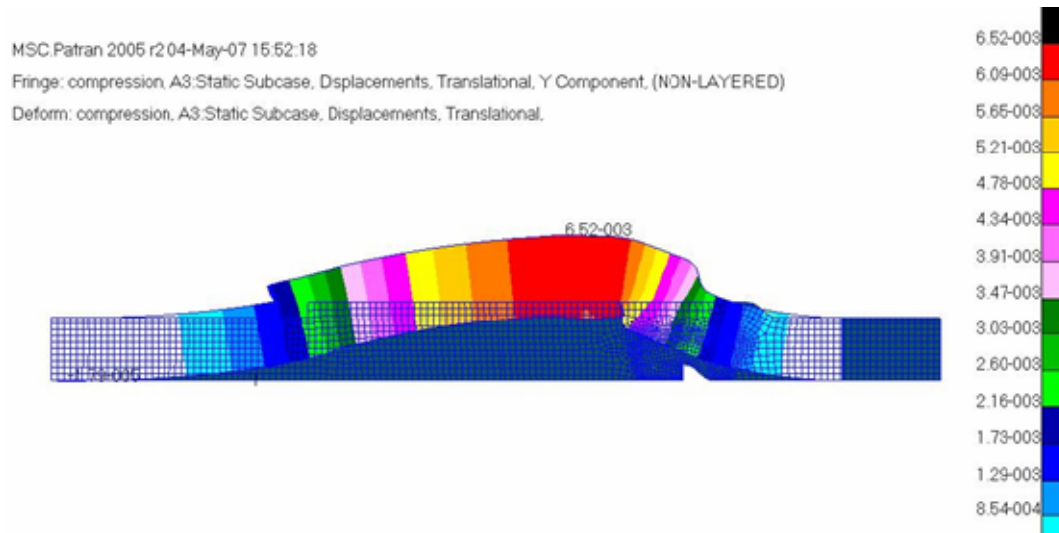
Figure 34.   Carbon Fiber Compression Model - displacement in the Y direction. Note the exaggeration; actual Y displacement is 0.00652".

48

As discussed in the previous section, experimental observations show that crack initiation within a scarf joint undergoing compression, is not always at the lower ply termination. Some failures have been observed initiating at the lower ply termination (just as in the tension case). Other failures have initiated in the center of the laminate where the fibers bend due to the lap joint. Failures have also been observed initiating at the center of the scarf and propagating out to the ply terminations. For this reason, three separate local models were built, one for each case.

1. Lower Ply Termination Crack Initiation

The lower ply termination model was essentially the same model as developed previously, with the geometry altered to match the carbon fiber test specimens. A global model was built, meshed, and a compressive load applied. Next, a more refined local model was built surrounding the area of interest (lower ply termination), and the boundary conditions were taken from the displacements within the global model. The crack closure method was used to determine the Energy Release Rate (ERR) and this rate was then compared with the load applied and the critical rates to predict failure.

Figure 35. Carbon Fiber Global Model – Note: local model is defined surrounding the lower ply termination.

49
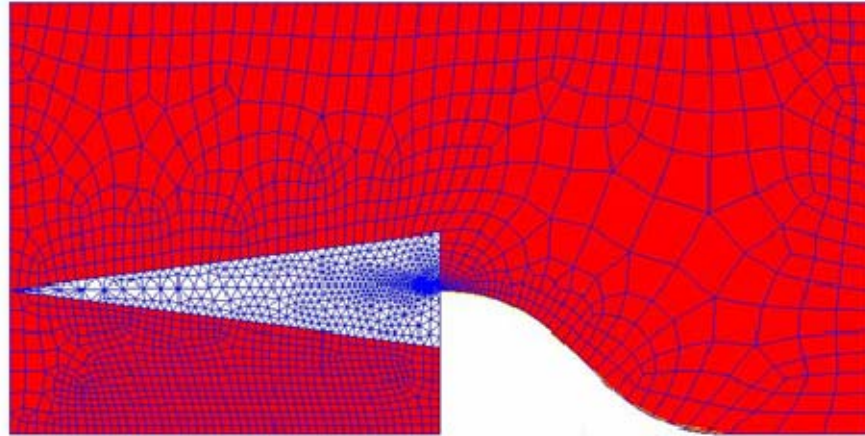
Figure 36.   Carbon Fiber Local Model at Lower Ply Termination – White represents the resin interface layer, which is 40% the thickness of an individual ply. Note the refined mesh surrounding the assumed initial crack.

2.   Center Thickness at Fiber Bend Crack Initiation

In order to attempt to model the mechanics within the scarf joint for the case where failure initiates at the center of the thickness away from the scarf, the local model was moved to this area of interest. Just as in the lower ply termination failure model, the local model for failure at the fiber bend was built with an assumed initial crack 0.254 mm long. Since this is a compression model, it is not possible to have a Mode I contribution at the lower ply termination, because the crack in that location is forced closed. However, in this case, the crack was placed in the center of the thickness where the global model indicated the largest Y-component of internal stress. This internal stress produced an opening effect on the crack, allowing for both Mode I and Mode II contributions to failure. Again, the crack closure was used to determine the ERR, and thereby predict the failure. The center crack was allowed to grow in each direction, in two separate cases, and the most critical crack growth direction was used.

Figure 37.   Carbon Fiber Global Model – Note: local model is defined surrounding the area where the fiber bends and delamination may initiate in the center of the thickness.

Fringe: compression, A1:Static Subcase, Stress Tensor, , Y Component, At Z2

High Y-Component of Internal Stress
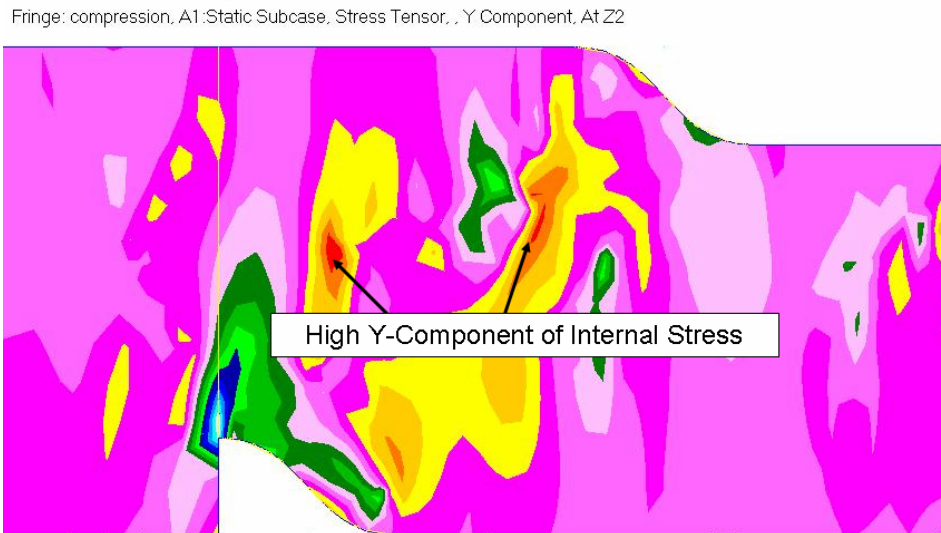
Figure 38.   Section of global model showing an elevated y-component of internal stress in the same location where the high speed camera captured crack initiation.
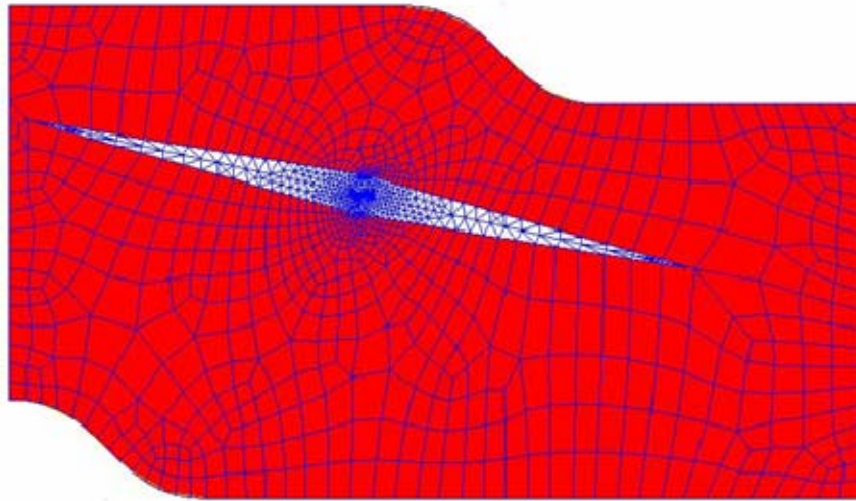
Figure 39.   Local model with resin layer, and initial assumed tapered crack, located at the center of the thickness in the area where the fibers bend. Resin layer shown in white.

3.   Crack Initiation at the Center of the Scar

In the third observed failure, delamination initiated at the center of the scarf joint, inside the secondary bond. The crack then propagated outward, toward the edges. For this case, the local model was centered on the scarf itself. The tapered initial crack and resin layer were applied just as in the previous model with the failure initiation at the center of the scarf.

Figure 40.   Carbon Fiber Global Model – Note: local model is defined surrounding the area where delamination may initiate at the center of the scarf.
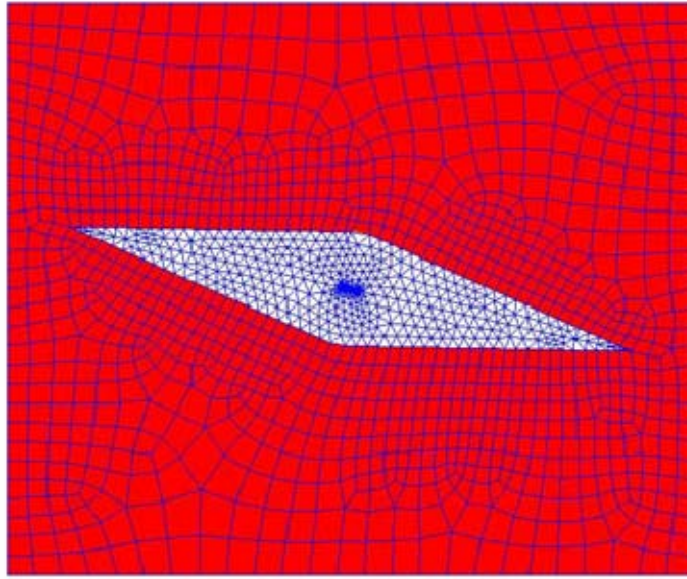
Figure 41.   Local model with resin layer, and initial assumed tapered crack, located at the center of the scarf. Resin layer shown in white.

C.   MODEL RESULTS

1.   Experimental Results

Thesis work conducted by Slaff included compression testing of scarf joints to failure.   The data from this testing was used as a comparison for the FE models developed. The geometry of the models was dictated by the tested specimens. These specimens were 16-ply, solid laminate, four ply-drops per step in the scarf, with a gage length of 120mm, a width of 38.1 mm and an approximate thickness of 8.5 mm. Five specimens were tested. The thickness of the specimens varied between 8.7 to 9.4 mm with an average value of 8.9 mm.

All carbon test specimens were designed with a length to thickness ratio so that buckling would not occur. All specimens were axially loaded in compression using constant displacement until failure. The failure loads were recorded and a high speed camera was used to capture fracture initiation and growth. The test results are detailed in Table 18.

Table 18.   Experimental Results of Carbon Fiber/Derakane Resin Compression Loading.   Note: specimen thickness varied due to hand lay up. (from Ref [23])

Experimental Data:	failure load	thickness
	(kN)	(mm)
Carbon 1	58.12	9.4
Carbon 2	50.18	9.0
Carbon 3	57.47	8.7
Carbon 4	55.20	8.8
Carbon 5	56.44	8.8
avg	55.48	8.9

2.   Model Predictions and Comparison

a.   Lower Ply Termination Model

The local model at the lower ply termination predicted compression failure at 57.85 kN. This is a 4.3% error based on the mean experimental value of 55.48. When the thickness of each specimen is factored in, the error is reduced even farther. The FE model was built with an assumed average thickness of 8.5mm. The specimen Carbon 3 is the closest to that thickness. Its failure load was failure load is 57.47 kN, giving a model error of only 0.7%. However, there is only one data point at this specific thickness, so the average failure load of all the specimens is best for comparison.
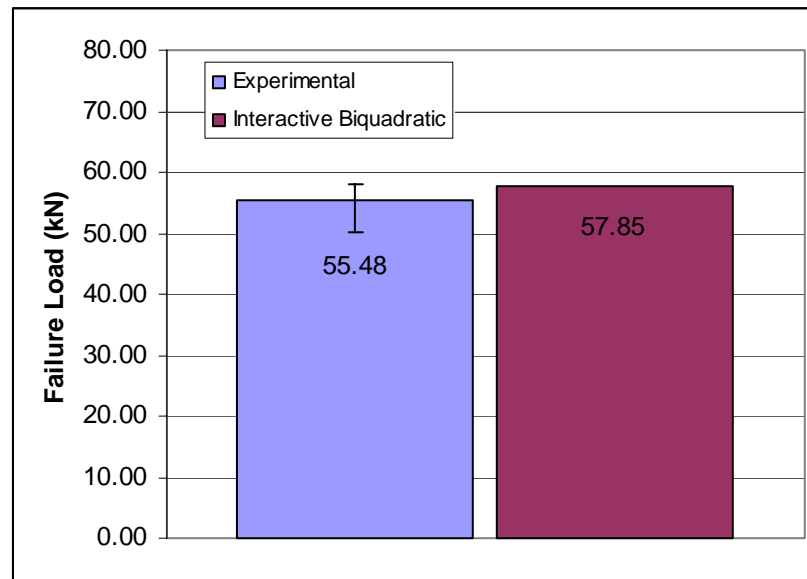
Figure 42.   Carbon Fiber Scarf Joint - Compression Failure Load vs. Predicted Failure Load

54
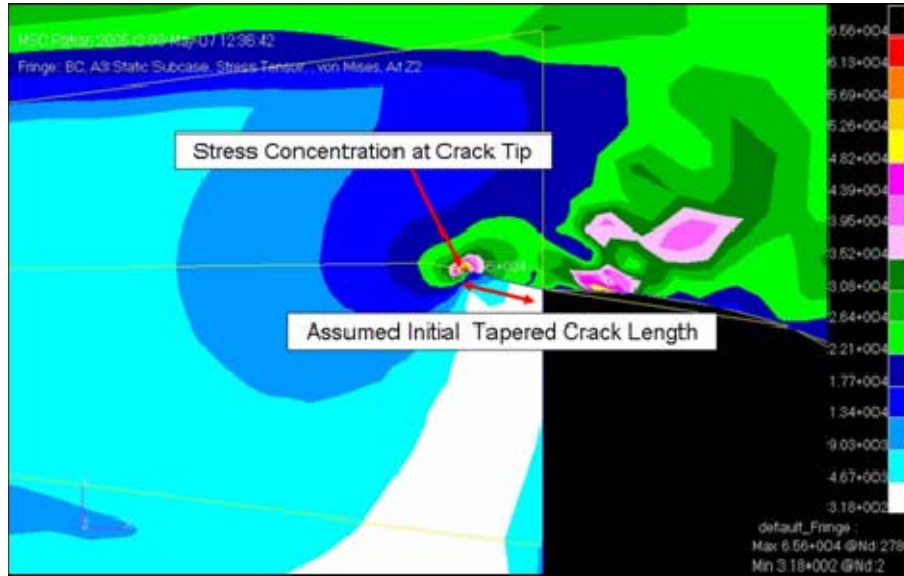
Figure 43.   Stress Concentration at Crack Tip – Section of the local model at the lower ply termination.

b.   *Center Thickness at Fiber Bend Crack Initiation Model*

The models with the crack initiation modeled at the fiber bend in the center of the specimen's thickness (in the area with the greatest Y-component of internal stress) were not successful. Even with the Mode I contribution due to crack opening, the predicted failure loads were two to three times greater than experimental results.

There are two potential causes for the poor prediction. First, the position of the assumed initial crack is vital to accurately predicting failure. Mode I forces are much more critical than Mode II when initiating delamination. In this model, the crack location was based on observations of crack initiation from a high speed camera, and on internal forces predicted within the global model. The area with the highest Y-component of stress in the global model seemed to correspond with the observations from the high speed footage, so the crack was placed there. The local model results showed that the crack opening forces were much too low for an accurate prediction and the internal stresses (fig 44) show the sensitivity of the placement of the crack. The crack must be placed exactly in the region of high stress.
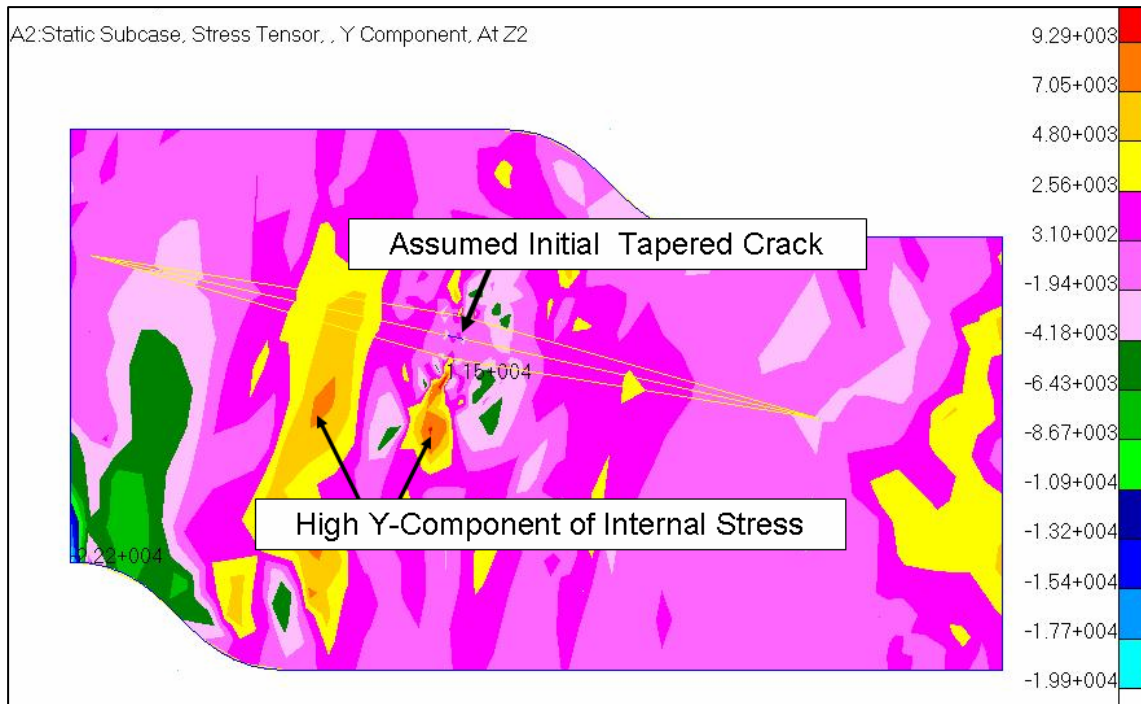
Figure 44.   Internal stresses within the local model. The greatest stresses are not in the regions of the greatest internal stress. Colors represent the Y-component of the internal stress.

The second potential cause for the poor failure predictions in the area of the fiber bend is that the specimens failed due to fiber buckling. The model is designed to predict failure based on delamination. Due to the bend in the fibers caused by the lap joint, the individual fibers in this region were as much as 45° off the primary loaded axis and, therefore, were much more susceptible to buckling. If the fibers buckled under the compressive load, it would cause the specimen to fail before delamination occurred. This is supported by the model's predictions of failure at two and three times greater load than was observed experimentally.

c.   *Center of Scarf Crack Initiation Model*

The attempt to predict scarf failure by relocating the local model, placing the initial assumed crack at the center of the scarf joint was also not successful. The crack in the center of the scarf did not experience significant opening, and therefore the

calculations to determine ERR by the crack closure method did not accurately predict failure. The model over-predicted the load that the joint could sustain by over one order of magnitude.

A different analysis technique may be needed to explain the mechanics of a failure that begins at the center of a scarf and propagates outward. A tapered initial crack within a modeled resin interface layer is an accurate method of predicting failure initiating at ply terminations, but not within the center of the scarf.

Another possible cause of the error in predicting failure initiating at the center of the scarf could be that when the test specimens were made, some air pockets were trapped at the center of the scarf or gaps were left at the interior ply terminations. The vacuum bagging technique was able to eliminate this porosity near the upper and lower surfaces, however, at the center of the joint, air remained trapped which concentrated stress weakened the joint. This possible cause of error is based on post-test observations of small air bubbles trapped within the composite.

THIS PAGE INTENTIONALLY LEFT BLANK

VI. CONCLUSIONS

It is possible to predict tensile and compressive failure within a composite scarf joint to a high degree of accuracy, if the proper modeling techniques are employed. Three different model types (isotropic, isotropic with resin interface layer, and orthotropic), two different initial assumed crack types (stepped and tapered), and seven variations of failure criteria (Mode I, Mode II, combined linear, mixed linear, mixed quadratic, bilinear, and interactive biquadratic) were evaluated to determine the combination which best predicts failure in a composite scarf joint.

A. TENSILE FAILURE PREDICTION MODEL

The best model for predicting tension failure in a composite scarf joint is the isotropic model with interface layer, using a tapered initial assumed crack path, and the Interactive Biquadratic failure criterion. The failure criterion should be tuned with an "m" value equal to -1.8 to most accurately represent the interaction between Mode I and Mode II.

This combination had an average magnitude error of 10% across all geometric variations tested.

B. COMPRESSION FAILURE PREDICTION MODEL

The best model for predicting compression failure in a composite scarf joint is also the isotropic model with interface layer, using a tapered initial assumed crack path, and the Interactive Biquadratic failure criterion. It is important to remember because $G_I=0$, the failure criterion is equal to the Mode II results for compression cases. Overall, this combination yielded accurate failure load predictions with an 8% magnitude error, when compared with experimental data.

When these analysis practices were applied to predict failure within a scarf joint built of the carbon fiber/vinyl ester resin material system undergoing testing for inclusion in the DDG-1000 deckhouse, compression failure was predicted with 4% difference from experimental results. This accuracy achieves the goal of this research. Designers can

apply these modeling techniques to predict failure analytically and, thereby, reduce the amount of experimental testing required prior to fielding composite technology.

C.   RECOMMENDATIONS

Recommendations for future work include:

1.   A sensitivity study to determine the effect material properties have on the failure predictions. This is especially necessary for energy release rate values which are experimentally determined and can have substantial deviations.

2.   Addition and refinement of out-of-axis loads for compression modeling to simulate eccentricity. The effect of these loads on Mode I failure when the initial crack is placed at the center of the scarf.

3.   Crack overclosure prevention in compression modeling by inclusion of spring elements across the crack or a contact surface on the crack faces.

4.   Detailed analysis of fiber buckling in the vicinity of the fiber bend due to the lap joint.

VII. APPENDICES

A. MATERIAL PROPERTIES COMPARISON

1. Material Properties Summary

Material	Density Lb/ft^3	Yield Strength Ksi	Young's Modulus Ksi	Fatigue Stress Ksi	Fire Resistance	1995 Costs $/Lb
ABS Grade A steel	491	34	29,600	20	Good	0.29
ABS Grade AH steel	491	55	29,600	20	Good	0.34
Aluminum (5086-H34)	166	16-22	10,000	10	Poor	1.65
Titanium	280	140	16,500		Fair	10.00
Sandwich Panel-LASCOR (stainless steel)	245-320	55	29,600	20	Good	
Composite Resins						
- Vinyl Ester	70	11-12	490		Poor	1.74
- Phenolic	72	5	530		Good	1.10
- Epoxy	75	7-11	530			3.90
Composite Fibers						
- E-glass	162	500	10,500			1.14
- S-glass	155	665	12,600			5.00
- Carbon-PAN	110	350-700	33-57,000			12.00
- Kevlar 49	90	525	18,000			20.00
Composite Cores						
- Balsa	7	1.3	370	N/A	Insulator	3.70
- Honeycomb Nx HRH-78	6	N/A	60	N/A		13.25

Material	Density Lb/ft^3	Yield Strength Ksi	Young's Modulus Ksi	Fatigue Stress Ksi	Fire Resistance	1995 Costs $/Lb
Composite Laminates - Solid Glass/Polyester - Solid Glass/Vinylester - Solid Carbon/Epoxy	96 90 97	20 50 88	1,400 3,000 8,700	Excellent fatigue life	Poor Fire Resistance – Good Insulator	2.50 3.50 10.00
Composite Sandwich - Glass/Poly Balsa Sandw. - Glass/VinE PVC Sandw. - Carbon/Epoxy Nomex	24 18 9			Excellent fatigue life	Poor Fire Resistance – Good Insulator	4.00 5.00 20.00

61

2.   Panels of Equal In-Plane Stiffness

Material	Skin Thick. (inch)	Core Thick. (inch)	Elastic Modulus (ksi)	Weight (lb/sqft)
Steel	0.08	0	30,000	3.36
Aluminum	0.25	0	10,000	3.62
E-Glass (0,90)	1.14	0	2,200	9.99
Kevlar (0,90)	0.60	0	4,200	4.49
Carbon (0,90)	0.35	0	7,200	2.87
Uni-E-Glass	0.57	0	4,400	4.99
Uni-Kevlar	0.30	0	8,400	2.24
Uni-Carbon	0.17	0	14,400	1.43
E-Glass/Core (0,90)	0.57	5	2,200	15.15
Kevlar/Core (0,90)	0.30	3	4,200	7.59
Carbon/Core (0,90)	0.17	1.75	7,200	4.68
Uni-E-Glass/Core	0.28	3	4,400	8.09
Uni-Kevlar/Core	0.15	1.5	8,400	3.79
Uni-Carbon/Core	0.09	1	14,400	2.47

* All panels have a stiffness of 2.5×10^6 pounds/inch

3.   Panels of Equal In-Plane Strength

Material	Skin Thick. (inch)	Core Thick. (inch)	Yield Strength (ksi)	Weight (lb/sqft)
Steel	0.19	0	80	7.56
Aluminum	0.26	0	58	3.74
E-Glass (0,90)	0.34	0	44	3.00
Kevlar (0,90)	0.25	0	60	1.89
Carbon (0,90)	0.14	0	105	1.18
Uni-E-Glass	0.17	0	88	1.50
Uni-Kevlar	0.13	0	120	0.94
Uni-Carbon	0.07	0	210	0.59
E-Glass/Core (0,90)	0.17	1.75	44	4.80
Kevlar/Core (0,90)	0.13	1.25	60	3.18
Carbon/Core (0,90)	0.07	0.75	105	1.96
Uni-E-Glass/Core	0.09	1	88	2.53
Uni-Kevlar/Core	0.06	0.5	120	1.46
Uni-Carbon/Core	0.04	0.5	210	1.11

* All panels have a maximum strength of 15.0×10^3 lbs/inch width

4.   Panels of Equal Flexural Stiffness

Material	Skin Thick. (inch)	Core Thick. (inch)	Mom. of Inertia (inch^4)	Weight (lbs/sqft)
Steel	0.74	0	0.0335	29.74
Aluminum	1.06	0	0.1004	15.39
E-Glass (0,90)	1.76	0	0.4543	15.46
Kevlar (0,90)	1.42	0	0.2386	10.71
Carbon (0,90)	1.19	0	0.1387	9.80
Uni-E-Glass	1.40	0	0.2262	12.25
Uni-Kevlar	1.13	0	0.1196	8.51
Uni-Carbon	0.94	0	0.0697	7.79
E-Glass/Core (0,90)	0.23	2	0.4539	6.04
Kevlar/Core (0,90)	0.16	1.75	0.2380	4.15
Carbon/Core (0,90)	0.15	1.375	0.1385	3.83
Uni-E-Glass/Core	0.15	1.75	0.2272	4.41
Uni-Kevlar/Core	0.13	1.375	0.1185	3.31
Uni-Carbon/Core	0.11	1.125	0.0692	2.96

* All panels have a stiffness (EI) of 1.0×10^6 pound-inch^2

5.   Panels of Equal Flexural Strength

Material	Skin Thick. (inch)	Core Thick. (inch)	Yield Strength (ksi)	Weight (lbs/sqft)
Steel	0.19	0	80	7.56
Aluminum	0.26	0	58	3.74
E-Glass (0,90)	0.34	0	44	3.00
Kevlar (0,90)	0.88	0	17	6.65
Carbon (0,90)	0.14	0	105	1.18
Uni-E-Glass	0.17	0	88	1.50
Uni-Kevlar	0.44	0	34	3.33
Uni-Carbon	0.07	0	210	0.59
E-Glass/Core (0,90)	0.12	1.25	44	3.47
Kevlar/Core (0,90)	0.20	2	17	5.09
Carbon/Core (0,90)	0.09	0.75	105	2.19
Uni-E-Glass/Core	0.09	0.875	88	2.46
Uni-Kevlar/Core	0.15	1.375	34	3.61
Uni-Carbon/Core	0.05	0.625	210	1.52

* All panels have a maximum moment capacity of 7.5×10^2 foot*pounds

THIS PAGE INTENTIONALLY LEFT BLANK

LIST OF REFERENCES

[1]   A.P. Mouritz, E. Gellert, P. Burchill, and K. Challis, "Review of advanced composite structures for naval ships and submarines," *Composite Structures,* Vol 53, pp. 21-41, 2001.

[2]   R. P. Ronnal, "Material selection for boats and ships," in Second International Conference Marine Applications of Composite Materials, 1988.

[3]   D. P. Johnson, "Experimental examination of secondarily-bonded stepped lap joints under quasi-static and fatigue loading." Mississippi State University, MSU-S.3b, 2001.

[4]   B. J. Jones, NSWCCD, (private communication), 2006.

[5]   D. P. Johnson, "Experimental examination of secondarily-bonded stepped lap joints under quasi-static and fatigue loading." Mississippi State University, MSU-S.3b, 2001.

[6]   S. W. Bartlett, NSWCCD, (private communication), 2007.

[7]   S. W. Bartlett, NSWCCD, (private communication), "Summary of unpublished scarf joint testing and analysis," 2007.

[8]   R. Krueger, "The Virtual Crack Closure Technique: History, Approach, and Applications," NASA Langley Research Center, NASA/CR-2002-211628, April 2002.

[9]   J. R. Reeder, "An Evaluation of Mixed-Mode Delamination Failure Criteria," NASA Langley Research Center, NASA/TM-1992-104210, February 1992.

[10]   MSC Software, Appl. "MSC.Patran 2005 r2 Installation and Operation Guide," 2004.

[11]   D. P. Johnson, "Experimental examination of secondarily-bonded stepped lap joints under quasi-static and fatigue loading." Mississippi State University, MSU-S.3b, 2001.

[12]   D. P. Johnson, "Experimental examination of secondarily-bonded stepped lap joints under quasi-static and fatigue loading." Mississippi State University, MSU-S.3b, 2001.

[13]   D. P. Johnson, "Experimental examination of secondarily-bonded stepped lap joints under quasi-static and fatigue loading." Mississippi State University, MSU-S.3b, 2001.

[14]   R. M. Jones, *Mechanics of Composite Materials*, New York: Hemisphere Publishing Corporation, 1975.

[15]   Ugural, Ansel and S. Fenster, *Advanced Strength and Applied Elasticity,* New Jersey: Prentice Hall, 2003.

[16]   M. Orlet and A. Caiazzo, "Analysis support of integral joint parametric testing," Material Sciences Corporation, Fort Washington, PA, SAR-029-99, 1999.

[17]   D. H. Mollenhauer, B. Fredrickson, G. Schoeppner, and E. V. Iarve, "Scarf-lap and step-lap joint repair in composite laminates: experimental and numerical examination," U.S. Air Force Research Laboratory, Dayton, Ohio, 2007.

[18]   C. Meyers, "Analyses of external doubler tests for evaluation of primary and secondary bonds in composite laminates," Material Sciences Corporation, Fort Washington, PA, MSC SAR-001-02, 2002.

[19]   K. K. Chawla, *Composite Materials: Science and Engineering.* New York: Springer, 1998.

[20]   S. W. Bartlett, NSWCCD, (private communication), "Summary of unpublished scarf joint testing and analysis," 2007.

[21]   S. W. Bartlett, NSWCCD, (private communication), "Summary of unpublished scarf joint testing and analysis," 2007.

[22]   B. J. Jones, NSWCCD, (private communication), 2006.

[23]   R. E. Slaff Jr., "The enhancement of composite scarf joint interface strength through carbon nanotube reinforcement," M.S. Thesis, Naval Postgraduate School, Monterey, CA, 2007.

[24]   B. J. Jones, NSWCCD, (private communication), 2007.

INITIAL DISTRIBUTION LIST

1. Defense Technical Information Center
   Ft. Belvoir, Virginia

2. Dudley Knox Library
   Naval Postgraduate School
   Monterey, California

3. Scott Bartlett
   Naval Surface Warfare Center, Carderock Division
   Code 651, Structural Systems Branch
   West Bethesda, Maryland

4. Brian Jones
   Naval Surface Warfare Center, Carderock Division
   Advanced Materials & Structures Branch
   Code 655, Structures & Composites Division
   West Bethesda, Maryland

5. Engineering and Technology Program Office
   Naval Postgraduate School
   Monterey, California

6. Tom and Sharon Greene
   Ridgefield, Connecticut